Journal of Asian Earth Sciences 249 (2023) 105612

Contents lists available at ScienceDirect

Journal of Asian Earth Sciences

journal homepage: www.elsevier.com/locate/jseaes

Petroleum system modelling in a compressional tectonic setting: The eastern Kuqa Depression, Tarim Basin, Northwestern China

Bing Wang [a,b,c], Nansheng Qiu [a,b,*], Ralf Littke [c], Sebastian Amberg [c,e], Zhengdong Liu [d]

[a] State Key Laboratory of Petroleum Resources and Prospecting, China University of Petroleum, 102249 Beijing, China
[b] College of Geoscience, China University of Petroleum, 102249 Beijing, China
[c] Institute of Geology and Geochemistry of Petroleum and Coal, Energy & Mineral Resources Group (EMR), RWTH Aachen University, 52064 Aachen, Germany
[d] Donghe Oil and Gas Development Department, PetroChina Tarim Oilfield Company, 84100 Korla, China
[e] Geological Institute, Energy & Mineral Resources Group (EMR), RWTH Aachen University, 52062 Aachen, Germany

ARTICLE INFO

Keywords:
Basin modelling
Petroleum system
Thermal maturity
Petroleum charge
Eastern Kuqa Depression

ABSTRACT

The eastern Kuqa Depression is part of a tectonically active foreland basin and hosts structure-related petroleum systems with Jurassic coals and Triassic lacustrine mudstones acting as source rocks. However, the relationship between the recent structural evolution and the development of petroleum systems is poorly understood. In this study, the paleo-geometries are restored by structural reconstruction based on a regional 2D seismic section. The geological evolution of the petroleum systems was modelled integrating structural restoration with basin and petroleum system model. Results show significant structural dependencies of the thermal history and hydrocarbon charge. Source rock thermal maturity in the Yangxia Sag and Dina Fold Belt in the south increased continuously since the onset of tectonic compression, whereas the maturity of the Yiqikelike Anticline in the north remained unchanged due to structural uplift. Hydrocarbon accumulations are modelled across different structural units, emphasising the control of tectonics on petroleum systems' development. Hydrocarbon accumulations occur mainly in structural traps located in the Dina Fold Belt and Dibei Slope. The present-day accumulations are characterised by multiple stages of hydrocarbon filling, during which the proportion of gas components was increasing. Finally, the different sources of hydrocarbons in various reservoirs are recognised and prospects are predicted. The fold- and fault-related traps and tight sand reservoirs in the Dina Fold Belt and Dibei Slope should be treated as prospective targets in the area. This study highlights the importance of integrating structural restoration and petroleum system modelling, which is particularly important for tectonically active basins.

1. Introduction

The Kuqa Depression is part of a Mesozoic-Cenozoic foreland basin located at the northern margin of the Tarim Basin (Lu et al., 1997). It is characterised by not only abundant petroleum reserves but also complex tectonic evolution that is considered a great challenge for exploration (Jia and Li, 2008). Recently, a series of major hydrocarbon discoveries have been reported in the eastern Kuqa Depression (Zhu et al., 2012; Wei et al., 2021). For example, gas production of the YN-2 well drilled in 1998 exceeded 100,000 m^3/d, indicating a significant potential for petroleum resources in the region. Other high-yield wells such as the DN-2, TZ-2, and TD-2 were drilled successively. However, the limited knowledge of petroleum systems due to complex tectonics has seriously impeded exploration and the search for favourable areas of petroleum.

Currently, one of the main exploration risks in the study area is related to regional differences in both the thermal maturity of source rocks and the hydrocarbon charge associated with local tectonic history. Previous works on the understanding of petroleum systems predominantly employed three categories of methods: thermal maturity measurements and thermal history simulation of source rocks (Li et al., 2008; Huang et al., 2019); stable carbon isotope and biomarker research on hydrocarbons (Liang et al., 2003; Zhao et al., 2005; Liu et al., 2011); and comprehensive analyses of fluid inclusions (Fan et al., 2014; Pang et al., 2019; Wan et al., 2022). Even though these methods are considered relatively reliable, there are typically space–time restrictions caused by the limited number of samples. In addition to the thermal

* Corresponding author at: State Key Laboratory of Petroleum Resources and Prospecting, China University of Petroleum, 102249 Beijing, China.
E-mail address: qiunsh@cup.edu.cn (N. Qiu).

https://doi.org/10.1016/j.jseaes.2023.105612
Received 31 August 2022; Received in revised form 13 January 2023; Accepted 6 March 2023
Available online 14 March 2023

maturity of source rocks, the processes of petroleum migration are still under discussion, and the relationship between petroleum systems development and tectonic evolution is not fully understood. Basin and petroleum system modelling (BPSM) is increasingly becoming a powerful tool for understanding the evolution of the basin's physical fields (e.g., temperature and pressure fields), source rock properties and hydrocarbon charge (Al-Hajeri et al., 2009; Neumaier et al., 2014). The modelling results can be compared and calibrated to real measurements from wells. Because BPSM is a dynamic modelling of geological processes on the full basin scale through time and accounts for their complex interrelationship, it can present a more holistic understanding of the development of petroleum systems (Hantschel and Kauerauf, 2009; Lipparini et al., 2021). In addition, geomechanics-based structural restoration can provide a framework for structure and stratigraphy over time. The integration of structurally restored models and BPSM can account for the effect of tectonic movement on petroleum systems (D'Ambrosio et al., 2021; Lipparini et al., 2021), and visualises the process of petroleum generation and migration (Burgreen-Chan and Graham, 2018), which is particularly important for the eastern Kuqa.

It is worth noting that there are some distinct discrepancies in petroleum system modeling between extensional and compressional tectonic settings. In extensional tectonics, where rocks move mainly in a vertical direction, an event-stepping method is typically employed to simulate the evolution of basin and petroleum system where vertical back-stripping approach is utilised to restore the paleo-geometries at each time step, and the depositional and erosion ages of the layers act as the time framework controlling the calculation steps (Hantschel and Kauerauf, 2009). However, for compressional tectonics, because repeated strata and strongly deformed rocks often occur due to horizontal compression, the conventional back-stripping approach would lead to geologically unreasonable paleo-geometries (Neumaier et al., 2014). Petroleum system development has strong dependencies on tectonic evolution. For example, structural histories and the resulting physical fields, such as temperature and pore pressure, as well as the evolution of the petroleum system (i.e. maturity of source rock, physical properties of reservoir rocks and hydrocarbon migration) in the various structural zones, may greatly differ within a basin. To address the above stated problems, a paleo-stepping method is selected where the paleo-geometries are predefined by the structural restoration technique and used as input for basin and petroleum system modelling. Structural reconstruction is implemented backwards in time by removing the syntectonic sediment layers, unfaulting sequentially and unfolding (the reverse of deposition and deformation), during which additional geometrical boundary conditions, including lateral movement and deformation of rocks, can be accounted for (Neumaier et al., 2014; Burgreen-Chan et al., 2016). Time steps in the intermediate reconstructed paleo-geometries control the time resolution of the basin and petroleum system model (Baur et al., 2009).

This study describes the thermal evolution of source rocks and hydrocarbon charge history in the eastern Kuqa Depression by an integration of 2-D structural restoration and BPSM. Structural effects on petroleum system development are examined, such as differences in petroleum generation, migration and accumulation caused by distinct local structural histories. Furthermore, the sources of main hydrocarbon

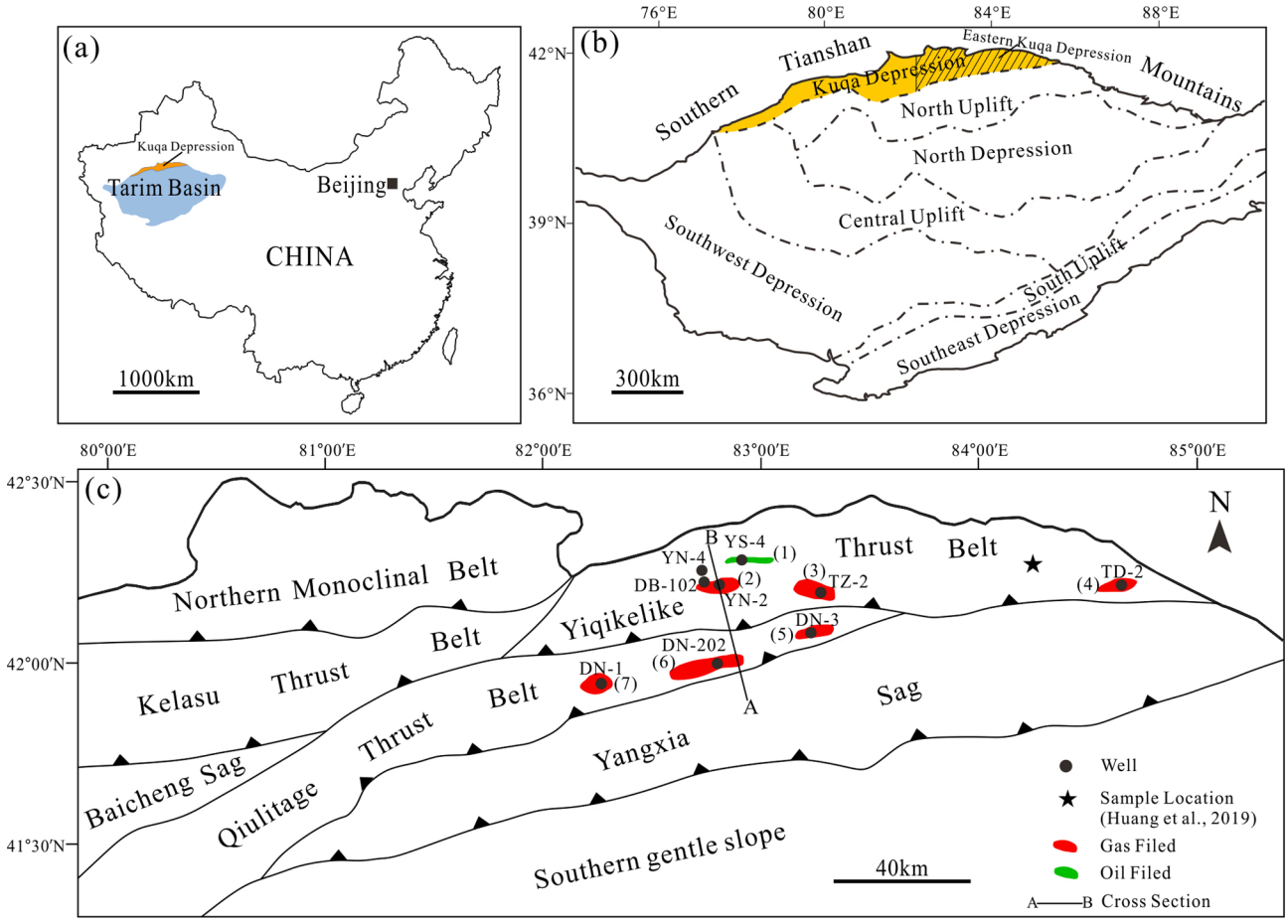

Fig. 1. (a) Geographical location of the Tarim Basin; (b) Tectonic units of the Tarim Basin and location of the Kuqa Depression at the northern margin (modified after Guo et al., 2016); (c) The eastern Kuqa Depression, including tectonic units, major oil and gas fields, sampled locations, and cross-section AB through the eastern Kuqa Depression. (1) = Yiqikelike oil field; (2) = Yinan2 gas field; (3) = Tuzi2 gas field; (4) = Tudong2 gas field; (5) = Dina3 gas field; (6) = Dina2 gas field; (7) = Dina1 gas field (modified after Guo et al., 2016; Qin et al., 2007; Huang et al., 2019).

accumulations and prospects are analysed. The study highlights the importance of tectonic evolution on petroleum systems in a tectonically active area.

2. Geologic setting

2.1. Structure and stratigraphy

The Kuqa Depression, located in the northern Tarim Basin, is bounded by the South Tianshan Mountains to the north and by the northern uplift to the south (Fig. 1; Jia and Li, 2008). This depression,

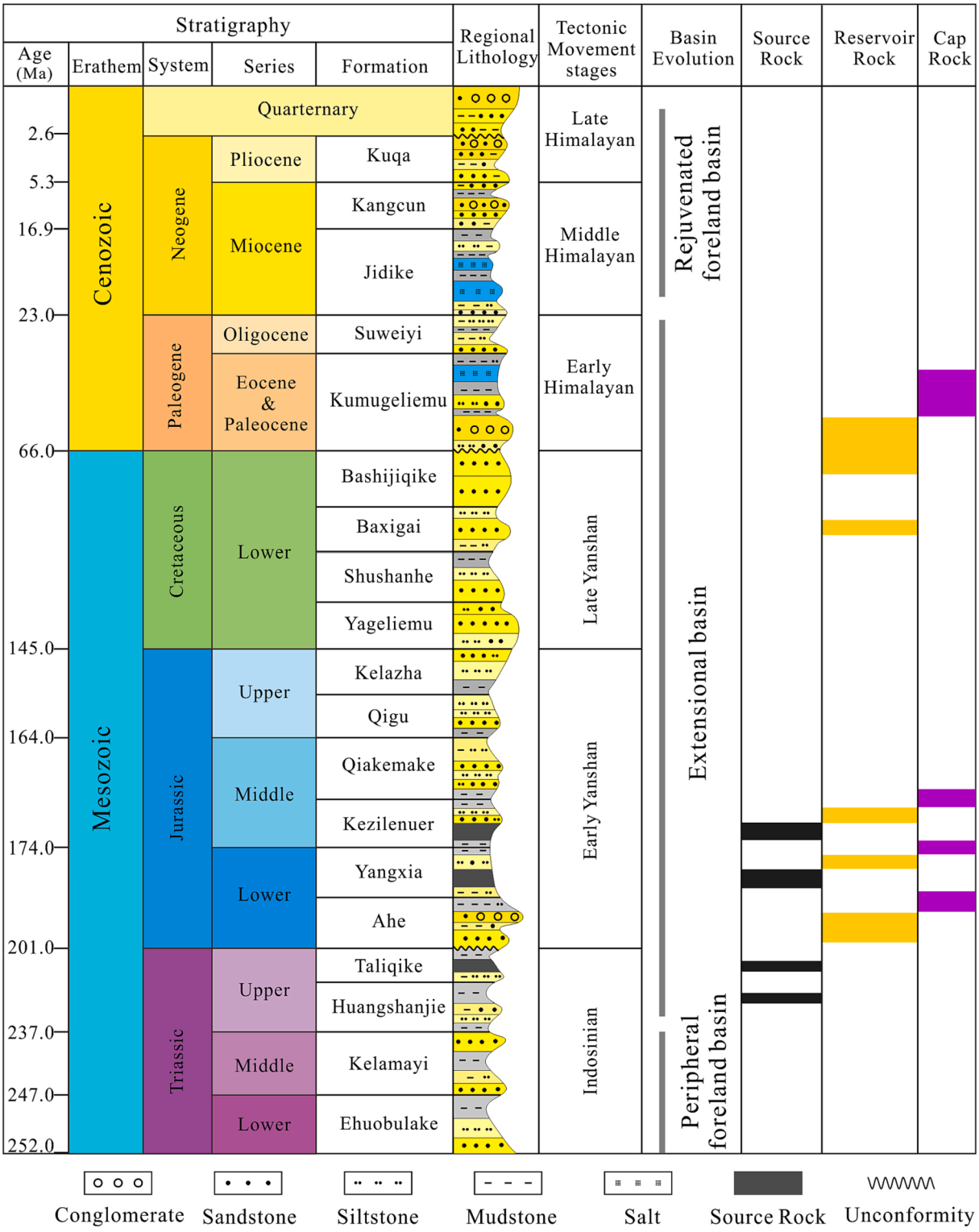

Fig. 2. Lithostratigraphy of the eastern Kuqa Depression (modified after Guo et al., 2016), showing key tectonic events, basin evolution, and the major petroleum system elements.

approximately 550 km long from east to west and 30–80 km wide from north to south, is the key hydrocarbon-producing area of the Tarim Basin. The Kuqa Depression is subdivided into several secondary structural units: the northern monocline belt, the Kelasu-Yiqikelike Thrust Belts, the Wushi-Baicheng-Yangxia Sags, the Qiulitage Thrust Belt, and the Southern Gentle Slope. The eastern Kuqa Depression refers to the area covering the Yiqikelike Thrust Belt, the eastern Qiulitage Thrust Belt (i.e., the eastern segment of the Qiulitage Thrust Belt) and the Yangxia Sag, and plays an important role in gas production.

The Kuqa Depression is part of a Mesozoic-Cenozoic foreland basin, which has experienced three tectonic phases associated with plate tectonics (Graham et al., 1993; Zeng et al., 2010). From the Late Permian to the Middle Triassic, an active orogenic belt along Tarim's northern margin created by a continent–continent collision, enabled the Kuqa Depression to enter the stage of a foreland basin (Allen et al., 1999). From the Late Triassic to Paleogene, the Kuqa Depression experienced post-orogenic extension with relatively weak tectonic movement and continuous subsidence and deposition (Lu et al., 1997). This phase was interrupted by regional uplift in the Kuqa Depression during the Late Cretaceous, caused by a convergence of several small blocks within the Tethys orogenic belt to the south of the Asia plate (Yang et al., 2002). Since the Neogene, the Indo-Asian collision rejuvenated the South Tianshan orogeny, and the depression began to evolve as part of a rejuvenated foreland basin (Yin et al., 1998). Structural styles were predominantly characterised by complex folds and thrust belts. Despite three main tectonic phases, the present-day geometry is shaped mainly by the phase of the rejuvenated foreland basin (Matte et al., 1996; Xiao et al., 2001), in which structural deformation occurred sequentially from the foothill zone to the interior of this depression (Yin et al., 1998; Wang et al., 2004): the northern monoclinal belt in the Early Miocene, the Kelasu-Yiqikelike thrust belts in the Late Miocene, and the Qiulitage Thrust Belt in the Pliocene. From the end of the Pliocene to the Quaternary, significant uplift and erosion took place on structural highs (e.g., the axis of the thrust belts), accompanied by the deposition of coarse sediments on structural lows (e.g. the sags; Li et al., 2012). Being influenced by the Neogene salt-bearing ductile rocks, the supra-salt and sub-salt strata have completely different structural deformation characteristics. Supra-salt structures include thrust faults and fault-related folds. Sub-salt structures are characterised by imbricated thrust belts, fault-related folds, and pop-up structures (Tang et al., 2004).

Influenced by the three tectonic stages mentioned above, the lowermost strata is of Upper Permian to the Middle Triassic age and composed of alternating shales, sandstones, and conglomerates with fan delta and lacustrine facies (Li et al., 2012). From the Late Triassic to the Jurassic, braided river, lacustrine, and swamp sediments were deposited in a warm and humid climate under the influence of a post-orogenic extensional regime (Huang et al., 2019). Lacustrine mudstones were developed in the Upper Triassic Taliqike Formation and major coal seams were deposited within the Lower Jurassic Yangxia Formation and Middle Jurassic Kezilenuer Formation, which are principal source rock layers. Sandstone units within the Ahe, Yangxia and Kezilenuer formations make up the principal reservoirs (Fig. 2; Liang et al., 2003; Zhao et al., 2005). During the Jurassic period, the main depocenter was located in the northern Kuqa Depression, and the corresponding strata were characterised by higher thickness in the north (Li et al., 2003). During the Early Cretaceous, the depocenter gradually moved southward, and sandstone-dominated sediments were deposited, followed by the absence of Late Cretaceous deposits due to regional uplift (Li et al., 2003; Jia and Li, 2008). With the resumption of subsidence at the beginning of the Paleogene, a fan delta sedimentary succession was deposited, as recorded by conglomerate-bearing sandstones at the base of the Kumugeliemu Group (Li et al., 2012), which forms another excellent reservoir in the eastern Kuqa Depression. In the following time, a lacustrine and evaporative system prevailed throughout the Kuqa Depression, leaving salt and shale interbedded with siltstone layers in the Kumugeliemu Group through Early Miocene Jidike Formation. Salt was mainly deposited in the Kumugeliemu Group in the western and central Kuqa Depression, while it is present in the Jidike Formation in the eastern Kuqa Depression, which provides regionally perfect seals for oil and gas traps (Zhuo et al., 2014).

2.2. Petroleum systems

Since the 1990s, seven large- and medium-sized oil and gas fields have been discovered in the eastern Kuqa Depression (Fig. 1c): Yinan2, Tuzi2, Tudong2 gas fields, and Yiqikelike oil field located in the Yiqikelike Thrust Belt; Dina1, Dina2 and Dina3 gas fields located in the eastern Qiulitage Thrust Belt (Zhao et al., 2015; Wei et al., 2021). In 2020, the predicted natural gas reserves in the eastern Kuqa Depression were estimated at 147.2 billion cubic meters and the oil reserves at 12.59 million tons (Wei et al., 2021). The reservoirs in the Yiqikelike Thrust Belt are within the Ahe, Yangxia and Kezilenuer formations, while the reservoir in the eastern Qiulitage Thrust Belt is located at the base of the Kumugeliemu Group. The reservoir rocks have distinct heterogeneity in petrophysical properties due to various diagenesis including compaction, cementation, dissolution and fracturing (Zhang et al., 2021). Variations in sandstone texture and grain composition led to different diagenesis evolution paths for reservoir rocks, resulting in great discrepancy in pore types and porosity. The observations of thin sections show that primary intergranular pores and intragranular dissolved pores comprise the dominant pore types with a very small fraction of microfractures (Fig. 3). Previous studies on sandstone samples suggest that porosities range from 1% to 12% with an average of about 7% (Zhang et al., 2021; Wang et al., 2018; Pang et al., 2019).

Comprehensive analyses of fluid inclusions indicated that there are two main episodes of hydrocarbon charge in the eastern Kuqa Depression: an early oil charge in the Miocene and late gas charge from the Pliocene onward (Liang et al., 2003; Li et al., 2014; Pang et al., 2019). Even though lots of studies on hydrocarbon sources have been performed, such as those based on stable carbon isotopes and biomarkers, there remains a dispute. Some researchers propose that oil mainly originated from the Jurassic coal seams (Qin et al., 2007; Liu et al., 2019; Wan et al., 2022); others consider that oil was generated from both the Triassic lacustrine mudstones and Jurassic coals (Fan et al., 2014; Song et al., 2019). There is a similar disagreement on gas sources as well, focusing on either generated from the Jurassic coal seams (Liang et al., 2003; Qin et al., 2007; Liu et al., 2019) or a mixture of the Jurassic coals and Triassic lacustrine mudstones (Zou et al., 2006; Fan et al., 2014; Song et al., 2019).

3. Methods

A combined approach of BPSM and structural restoration has been used to reconstruct the histories of thermal maturity and hydrocarbon charging in the eastern Kuqa Depression. As a dynamic tool, the BPSM can fully simulate the generation, migration, accumulation and dissipation of hydrocarbons in a petroleum system through geologic time (Hantschel and Kauerauf, 2009). The BPSM was performed using PetroMod Teclink 2D with inputs including stratigraphic and structural framework, lithological facies, stratigraphic ages, source rock properties, paleo basal heat flow, paleo water depth (PWD) and sediment–water interface temperature (SWIT).

3.1. 2D structural restoration

Structural restoration is considered a very important part of the BPSM because the resulting paleo-geometries through geological time can provide a more realistic basin history and be employed to compute the generation and migration of hydrocarbons (Burgreen-Chan et al., 2016; D'Ambrosio et al., 2021). Structurally reconstructed models go back in time from a present-day geometry by removing sequentially older sediment layers, restoring faults, unfolding structural deformation

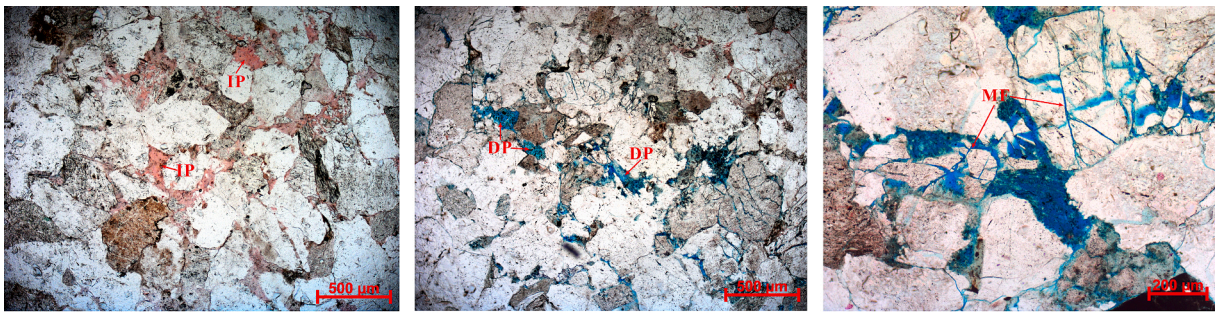

Fig. 3. Thin section images of sandstones showing pore types. (a) Sample 4785.5 m, well YN-2, plane-polarised light, primary intergranular pores (IP). (b) Sample 4782.6 m, well YN-2, plane- polarised light, dissolved pores (DP). (C) Sample 5092.5 m, well DB-102, plane- polarised light, microfractures (MF). See Fig. 1c for the locations of wells YN-2 and DB-102.

and decompacting the underlying sediments at each successive time step (Hantschel and Kauerauf, 2009). A N-S-oriented seismic line through the study area was selected as a present-day input for the structural restoration. This 2D section can be subdivided laterally into the Yangxia Sag, the Dina Fold Belt, the Dibei Slope, and the Yiqikelike Anticline based on their distinct structural histories (Fig. 4).

The technique of balancing cross-sections based on geometry and kinematics is traditionally used to perform structural restoration, which follows strict geometric assumptions such as preservation of the area, minimisation of deformation, of changes in segment length or minimisation of shearing, constant fault slip, fixed faults in space, or discontinuous rigid blocks (Maerten and Maerten, 2006). However, these basic assumptions are not suitable to compute fault block deformation, fault-slip distributions and potential interactions of different sets of faults during a given tectonic stage (King et al., 2010). To obtain a more realistic tectonic evolution model, a numerical tool based on a finite element method (FEM), Dynel 2D, has been utilised for structural restoration in this study. This tool uses physical principles of the conservation of mass and momentum that control rock deformation and linear-elastic theory for a replacement of kinematic and geometric assumptions. Rock mechanical properties (e.g., bulk modulus, Poisson's Ratio) are assigned as input parameters to gain a more natural deformation process (Maerten and Maerten, 2006).

In this study, each restored paleo-model represents a key time step in tectonics or hydrocarbon charge evolution. Some uncertainties exist in the restoration. For example, the timing and displacement of faulting and magnitude increment of folding at a single time interval is hard to constrain due to limited calibrated data. The obtained paleo-geometries have been treated as carefully as possible to honor the overall basin history. Additionally, rock mechanical parameters, such as the Young's Modulus and Poisson's Ratio, are assumed to be homogeneous in a single layer.

3.2. Modelling

3.2.1. The restored structural model

This section describes the structural history of the eastern Kuqa Depression since the Neogene, derived from the structural restoration.

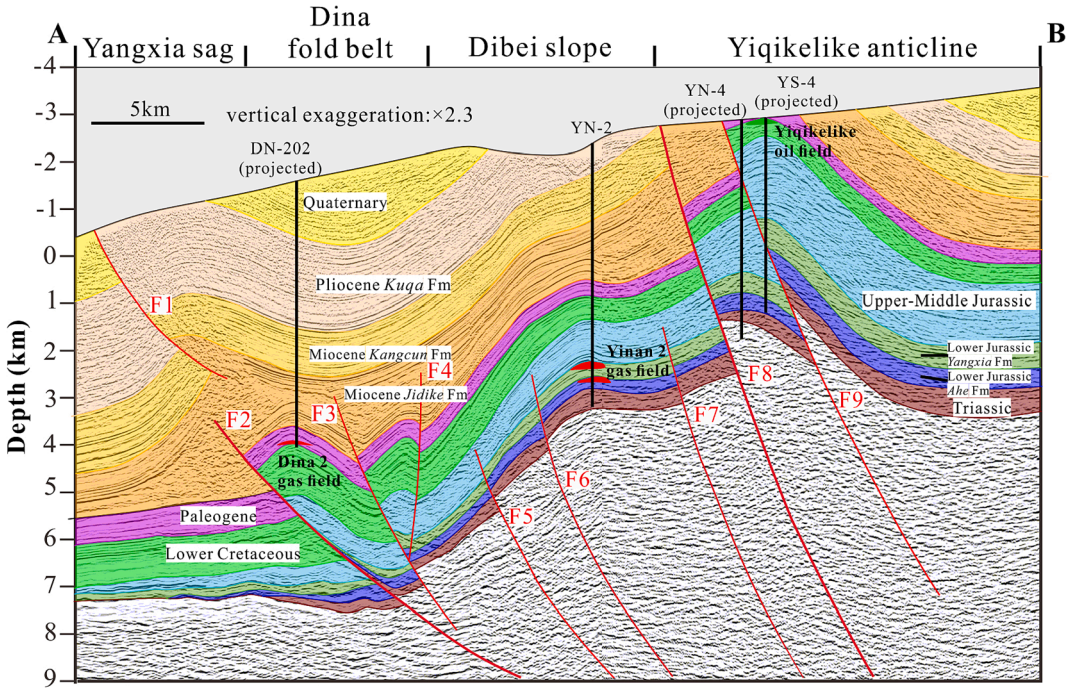

Fig. 4. Stratigraphy and structure of the selected 2D seismic line interpreted by Tarim Oil Field Company (2022) with the tectonic subunits and the corresponding names of layers and faults. Four wells (DN-202, YN-2, YN-4, YS-4) are passing through or are located close to the seismic line. The Dina Fold Belt is located in the eastern Qiulitage Thrust Belt; the Dibei Slope and Yiqikelike Anticline belong to the Yiqikelike Thrust Belt.

Although the paleo-geometries before the Neogene have also been put into the BPS model, they are not our study focus and, therefore, not displayed herein. The structural history can be divided into four-time steps. (1) During the Jidike Formation deposition (Fig. 5a-b), compression from the Southern Tianshan mountains only led to weak deformation; an initial Yiqikelike Anticline with a low amplitude began to form. Two preexisting reverse faults (i.e., F2 and F8) developed during the Late Permian to Middle Triassic were reactivated. (2) During

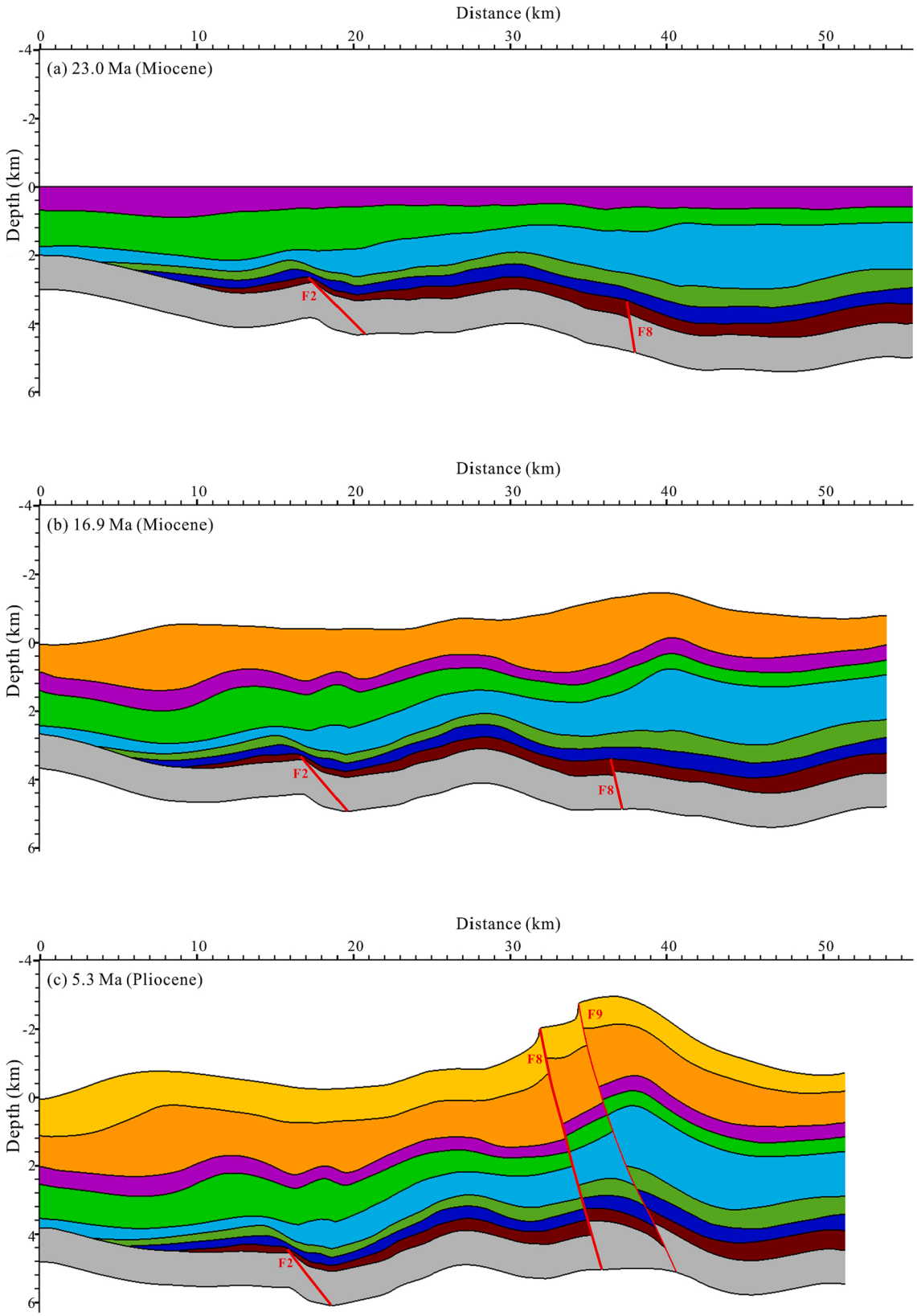

Fig. 5. Structurally restored models of the selected section using Dynel 2D, showing the evolution of strata and structure during the rejuvenated foreland basin stage.

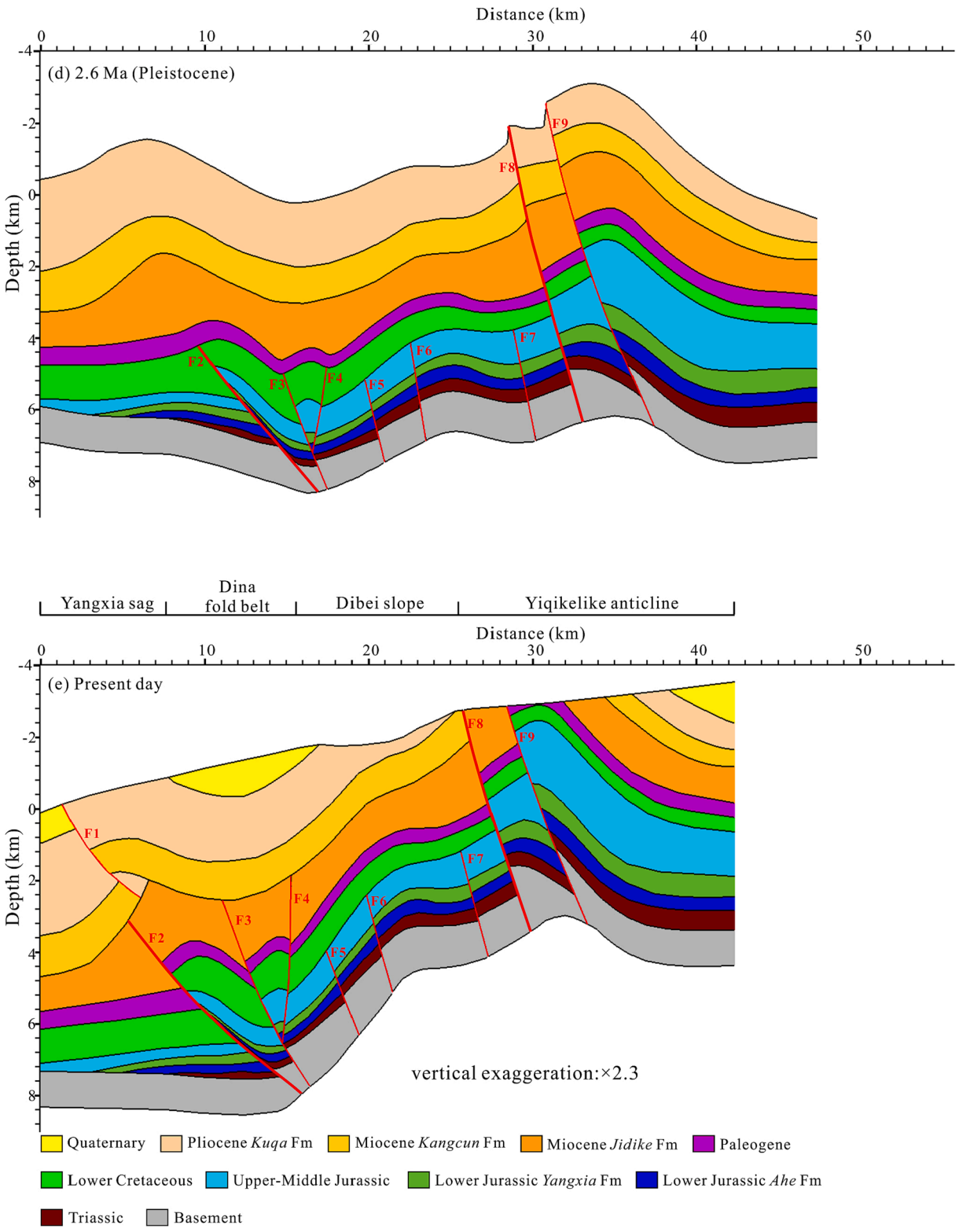

Fig. 5. (*continued*).

the Kangcun Formation deposition (Fig. 5c), increasing compression enhanced the Yiqikelike Anticline. The fault F8 and the freshly-formed fault F9 cut through this transect vertically. (3) During the Kuqa Formation deposition (Fig. 5d), deformation continued to spread southward, accompanied by the occurrence of the Dibei Slope and the Dina Fold Belt. Some freshly-formed faults divided the Mesozoic section into several blocks and even a pop-up structure (the block between F3 and F4). A combined effect of folding and thick deposition produced a significant burial increment for the source rocks. It is important to note that, as mentioned in the geologic setting section, the most significant uplift and erosion on structural highs occurred from the end of the Pliocene to the Quaternary (i.e., since 2.6 Ma). Therefore, during the structural restoration, we assumed that no erosion event occurred on structural highs before 2.6 Ma, although this simplification may cause

uncertainties in the basin geometry. (4) During the Quaternary (Fig. 5e), strong compression resulted in a significant uplift and erosion in the Yiqikelike Anticline, while both the Dina Fold Belt and Yangxia Sag experienced continued subsidence. Meanwhile, inclination of the formations at the Dibei Slope reached the maximum. The debris eroded from the structural highs was redeposited to form the Quaternary layer in the structural lows. From the Neogene to the present day, the total shortening of the section is estimated to reach approximately 13.4 km, accounting for 24% of the original section prior to tectonic compression.

Based on paleo-basin geometries derived from the structural restoration, a 2D BPSM has been built in the eastern Kuqa Depression to reconstruct the histories of thermal maturity and hydrocarbon charge. Four wells of DN-2, YN-2, YN-4, and YS-4 provide thermal calibration parameters, such as measured temperatures and vitrinite reflectance of source rocks. Vitrinite reflectance was calculated using the "Easy% R_o" method of Sweeney and Burnham (1990). The combined migration model, a combination of Darcy and invasion percolation migration approaches, is used to model the petroleum migration in this study. The basin model is divided into domains with high or low permeabilities. In low-permeability lithologies, the Darcy migration approach is used to model flow, in which the migration is driven by the hydraulic pressure gradient, buoyancy, and capillary pressure. In high-permeability lithologies, the invasion percolation migration approach is applied, which only considers buoyancy and capillary pressure of rocks and is particularly suitable for complex geometry (Baur et al., 2011). Compared to the Darcy approach, the invasion percolation calculates the invading process of petroleum for each cell instantaneously, which greatly decreases simulation runtimes (Baur and Katz, 2018). The threshold at which invasion percolation is switched to the Darcy approach is set to a value of 10^{-2} mD at 30% porosity of the corresponding lithology, which has been proven to work well in many basins (Hantschel and Kauerauf, 2009). It is important to note that the instantaneous invasion means that hydrocarbon viscosity is ignored in secondary migration, which is considered an acceptable approximation in geologic conditions because the flow rate is slow enough that the viscous effect can be neglected (England et al., 1987). Because of the rough stratigraphical divisions in the restored models, especially for major lithostratigraphic units, splitting of the following layers was done to distinguish the source rocks, reservoirs and overburden or underlying layers in a single formation (Fig. 6). Lithology (see Table 1 for detailed description) and average thickness proportion of each newly split sublayer are respectively from cuttings and well top markers from YN-2, YN-4 and YS-4:

1. The Triassic was split into three layers: the top 20% for the Taliqike Formation, the middle 40% for the Huangshanjie Formation, and the bottom 40% for the Middle and Lower Triassic.
2. The Yangxia Formation was split into three layers: the top 40% for the reservoir layer, the middle 30% for the source rock layer, and the bottom 30% for the basal layer.
3. The Middle and Upper Jurassic was split into four layers: the top 30% for the layer, including the Upper Jurassic and Qiakemake Formation, the next 40%, 15% and 15% for the reservoir layer, source rock layer and basal layer of Kezilenuer Formation, respectively.
4. The Paleogene was split into two layers: the top 85% for the sealing layer and the bottom 15% for the reservoir layer.

3.2.2. *Source rocks and kinetics*

For our model, three sets of source rocks were assigned: coals in the Kezilenuer and Yangxia formations and lacustrine mudstones in the Taliqike Formation, which are all characterised by Type III kerogen (Liang et al., 2003; Zhao et al., 2005). Indicated by outcrop samples of Jurassic coals with a $\%R_o$ range of 0.58–0.66 in the eastern Kuqa Depression, the measured total organic carbon (TOC) and hydrogen index (HI) are as high as 70 wt% and 185 mg HC/g TOC, respectively (Huang et al., 2019), which can be approximated as the initial values due to the low maturity. However, well data show that coals only account for a small part of corresponding formations (Table 1). To reflect the total volume percentage of coals in the entire layer, an average TOC content calculated from the lithology mixture ratio was assigned: a TOC of 18.7 wt% for the Kezilenuer Formation coal and 22.5 wt% for the Yangxia Formation coal. In the same way, the Triassic mudstone source rocks were calculated to have an average TOC of 3 wt% and HI of 150 mg HC/g TOC.

Previous studies suggested that coal produces predominantly gas

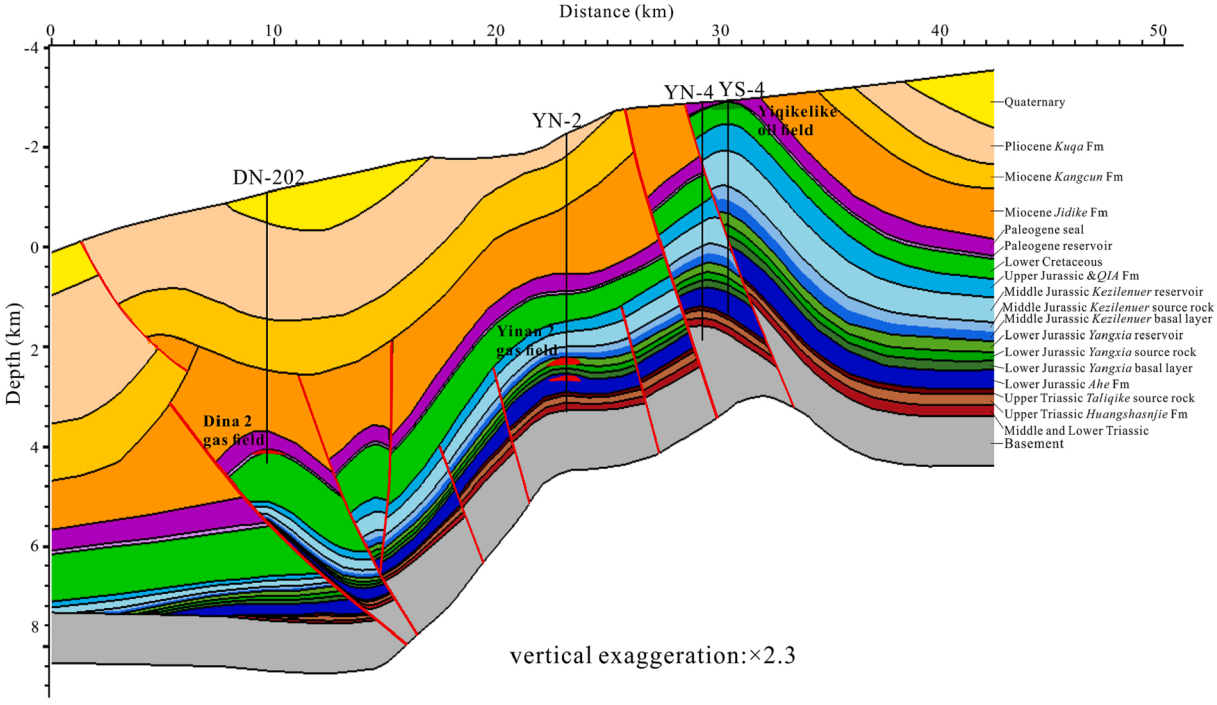

Fig. 6. The cross-section showing subdivided layers with petroleum system elements including the source rocks, reservoir intervals, and cap rocks. Lithology for each layer is present in Table 1. QIA = Qiakemake.

Table 1
Assigned lithologies and corresponding petrophysical parameters.

Layer	Litho mixture ratio (%)	Initial porosity (%)	Compressibility (GPa^{-1})		Permeability (log mD)		Thermal conductivity (W/m/K)		Heat capacity (kcal/kg/ K)		Poisson's Ratio	Bulk Modulus (GPa)
			min.	max.	at 1% por.	at 25% por.	at 20℃	at 100℃	at 20℃	at 100℃		
Quaternary	30cg 50ss 20sh	43.5	1.65	98.65	−3.44	1.5	2.82	2.58	0.20	0.23	0.23	From compaction curve
Pliocene *Kuqa* Fm	10cg 55ss 35sh	50	2.13	157.67	−4.25	0.8	2.75	2.51	0.20	0.24	0.22	
Miocene *Kangcun* Fm	5cg 60ss 35sh	50.6	2.14	158.34	−4.2	0.85	2.83	2.59	0.20	0.24	0.22	
Miocene *Jidike* Fm	5ss 15sil 25sh 55sa	28.35	1.38	117.73	−11.96	−9.55	3.78	3.34	0.21	0.24	0.48	0.5
Paleogene seal	20ss 20sil 50sh 10sa	54.3	2.67	227.85	−7.48	−2.7	2.35	2.25	0.21	0.24	0.26	From compaction curve
Paleogene reservoir	20cg 80ss	37.7	1.07	23.49	−2.1	2.7	3.36	2.96	0.20	0.23	0.22	
Lower Cretaceous	70ss 15sil 15sh	47.45	1.73	95.26	−3.48	1.5	3.14	2.79	0.21	0.24	0.23	
Upper Jurassic & *QIA** Fm	10ss 20sil 70sh	64.1	3.36	305.76	−7.4	−2	1.87	1.86	0.21	0.24	0.25	
Middle Jurassic *Kezilenuer* reservoir	60ss 30sil 10sh	48.1	1.73	87.89	−3.82	1.2	2.97	2.67	0.21	0.24	0.23	
Middle Jurassic *Kezilenuer* source rock	20sil 55sh 25co	68.5	16.75	2427.7	−7.8	−2.47	1.12	1.31	0.31	0.36	0.30	
Middle Jurassic *Kezilenuer* basal layer	20sil 80sh	67	3.65	343.34	−8.07	−2.6	1.71	1.75	0.20	0.24	0.25	
Lower Jurassic *Yangxia* reservoir	65ss 20sil 15sh	48.15	1.77	99.07	−3.7	1.3	3.28	2.89	0.21	0.24	0.23	
Lower Jurassic *Yangxia* source rock	20sil 50sh 30co	68.8	19.38	2844.5	−7.77	−2.44	1.03	1.25	0.31	0.36	0.32	
Lower Jurassic *Yangxia* basal layer	5ss 25sil 70sh	64.8	3.79	348.18	−7.62	−2.2	1.19	1.36	0.22	0.26	0.25	
Lower Jurassic *Ahe* Fm	15cg 75ss 10sh	42.25	1.4	63.06	−2.62	2.25	3.34	2.94	0.20	0.23	0.23	
Upper Triassic *Taliqike* source rock	30sil 70sh	65.5	3.45	313.37	−7.85	−2.4	1.75	1.78	0.31	0.36	0.28	
Upper Triassic *Huangshanjie* Fm	10ss 25sil 65sh	63.35	3.25	290.77	−7.29	−1.9	1.89	1.88	0.21	0.24	0.23	
Middle and Lower Triassic	30ss 20sil 50sh	58.3	2.78	230.6	−6.06	−0.8	2.23	2.13	0.21	0.24	0.21	
Basement	100 limestone	48	1.88	68.65	−1.99	0.72	2.30	2.18	0.20	0.23	0.22	

* QIA = Qiakemake.
cg = conglomerate; ss = sandstone; sil = siltstone; sh = shale; sa = salt; co = coal.

with some oil (Littke and Leythaeuser, 1993; Froidl et al., 2020). Confined pyrolysis experiments (gold capsules) also showed that coals in the study area have a potential for oil generation (Huang et al., 2019). The timing and components of hydrocarbon generation can be quantified by kerogen kinetics, typically described by a series of sequential and parallel reactions (Hantschel and Kauerauf, 2009). Our 2D model

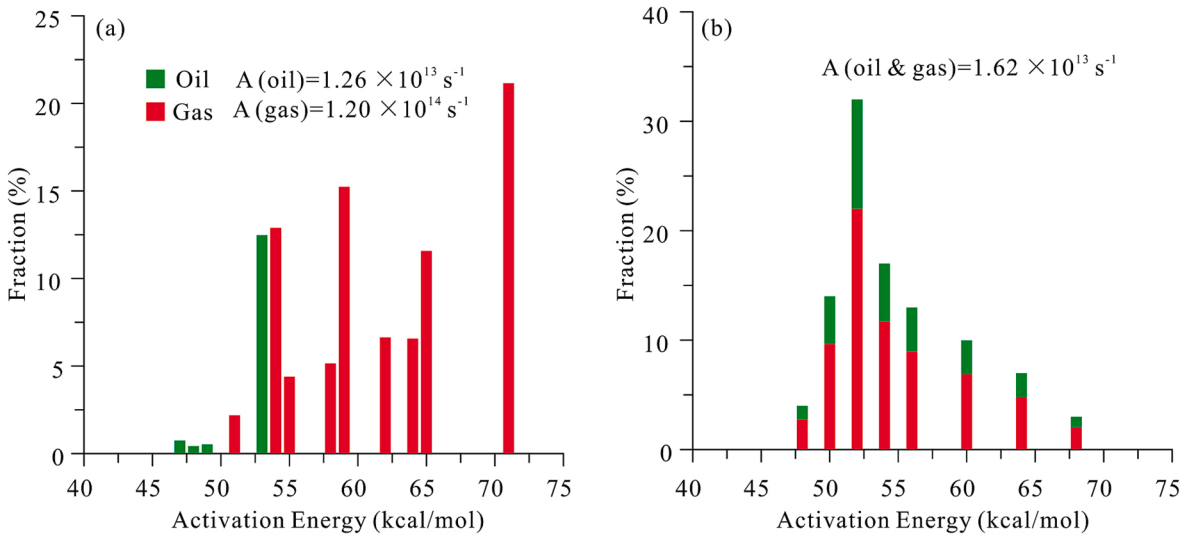

Fig. 7. Oil-gas kinetic models for the Jurassic coals (a) from Huang et al. (2019) and the Triassic mudstones (b) from Burnham (1989). A = frequency factor in 1/s.

employed oil–gas kinetic models for all source rocks. For the coals in the Kezilenuer and Yangxia formations, a distribution of activation energies and a pre-exponential factor (Fig. 7a) obtained from low-maturity coal samples in the study area (Huang et al., 2019) were assigned. For the lacustrine mudstone in the Taliqike Formation, a standard Type III kinetic model based on Burnham (1989) was selected (Fig. 7b).

3.2.3. Lithology input

Table 1 shows the lithologies and corresponding physical properties used in the BPSM. The lithological mixture for each layer is derived from the cuttings from key wells located on or close to the modelled section. Because only a few wells have penetrated the depression basement due to its large burial depth, a layer of about 1000-m-thick limestones acted as the basement of the 2D model based on the knowledge of pre-Triassic strata in the North Uplift, Tarim Basin.

Under consideration of the proportion of the mixed components, the petrophysical properties of the mixed lithologies were first calculated from the mean values of the mixed components and were then calibrated with well data. The properties of each single component were derived from a comprehensive literature review (Wang et al., 2005; Hantschel and Kauerauf, 2009; Zeng et al., 2010; Wang et al., 2022). It is worth noting that diagenetic heterogeneity and the resulting discrepancy in petrophysical properties cannot be simulated due to the limitations of the model in this study, although they may affect hydrocarbon charge. Nevertheless, this model can still be used to reconstruct petroleum migration process and estimate prospective targets on the basin scale. In addition, a simplified fracture model based on the Griffith theory was used in which fracturing occurs when pore pressure exceeds the defined fracture pressure. The fracture threshold for all lithologies was defined as 80% of the difference between lithostatic and hydrostatic pressures, except a ratio of 90% for the salt-bearing rocks in the Jidike Formation.

3.2.4. Boundary conditions and fault properties

The thermal boundary conditions are usually prescribed to reconstruct the thermal history of a basin, typically including surface temperature at the top of the model, basal heat flow at the base of model, and no heat flow crossing the model sides through geological time (Hantschel and Kauerauf, 2009). For this simulation, surface temperature over time was calculated from the global mean paleotemperature model proposed by Wygrala (1989). Various paleothermometers indicated that the Tarim Basin experienced a decreasing heat flow from the Mesozoic to the Cenozoic (Qiu et al., 2012). A heat flow of 64 ~ 56 mW/m^2 during the Mesozoic and 56 ~ 45 mW/m^2 during the Cenozoic was assigned (i.e., best-fit scenario in Fig. 8). The maximum value occurred at the onset of the extensional basin stage (i.e., the end of the Triassic) and the present-day heat flow decreased to 45 mW/m^2 due to the strong overthrusting movement occurring during the Cenozoic. This scenario is the combined result of paleo heat flow recorded by the paleothermometers (Li et al., 2010; Tang et al., 2014) and thermal calibration (see Fig. 9). It is worth noting that for modelling studies in basin-scale areas with rugged topography, the sea level rather than the sediment surface is typically defined as the hydrostatic zero level (Hantschel and Kauerauf, 2009), since the sediment surface varies greatly over a basin, especially for tectonically active areas. The hydrostatic pressure is then equivalent to the weight of the water column measured from the sea level; it has a positive value below and a negative value above sea level (Fig. 9). In fact, a difference between the pore pressure and hydrostatic pressure above the sea level is referred to as the groundwater potential in the field of hydrogeology, which is synonymous with overpressure and usually induces topographic driven flow near the sediment surface.

The faults were set open in the paleo geologic time and closed at the present day based on the fault activities as shown in the structural restoration. The opening of the faults in paleo geologic time allows fluid to flow along and across faults in the model, which was also suggested by the vertical hydrocarbon migration along faults in the study area during the thermally-mature period (Lu et al., 2016; Pang et al., 2019); the closed faults at the present day prevents fluid transmission related to faults in the model, indicated by both the observed fault-related traps and pressure compartments (Zhou, 2001; Fu et al., 2015).

3.2.5. Calibration data

The calibration data in this study comprise the measured temperatures, pressures and vitrinite reflectance (%R_o) and were taken from unpublished well reports and experiment database from Tarim Oil Company. The measured well temperatures and pressures were obtained from drill stem tests (DSTs), considered highly reliable data (Förster et al., 1997). Since the pressures from DSTs are usually distributed only in reservoir rocks, mud weights are used for a rough estimate for pore pressures. Vitrinite reflectance (%R_o) applied in the 2D model includes two types of data: the measured ones and the equivalent ones converted from the Rock-Eval parameter T_{max} (the temperature at which the maximum rate of hydrocarbon generation occurs during pyrolysis analysis) using the rule documented by Jarvie and Lundell, (2001):

$$\%R_o \text{ (converted)} = 0.018*T_{max}\text{-}7.16$$

Because this is an empirical formula based on a high number of source rocks with Type II or III kerogens in Texas (Jarvie and Lundell, 2001), the equivalent %R_o calculated from T_{max} should be regarded as a broad estimate of maturity.

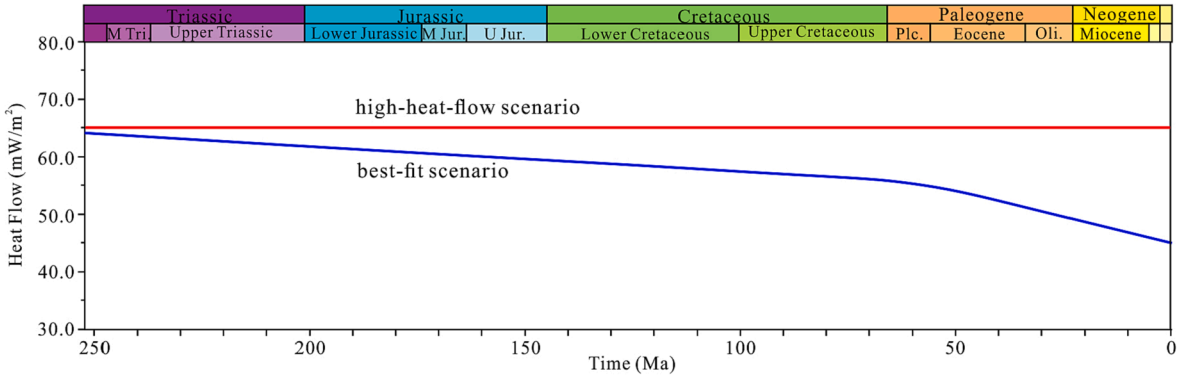

Fig. 8. The scenarios of basal heat flow through time used in this study. The best-fit scenario, showing a decreasing thermal regime from the Mesozoic onward, was calibrated to the present-day temperatures and maturities and has the best fit with the measurements. The high-heat-flow scenario, a time-constant value of 65 mW/m^2, was used to test the heat flow sensitivity to the modelled source rocks.

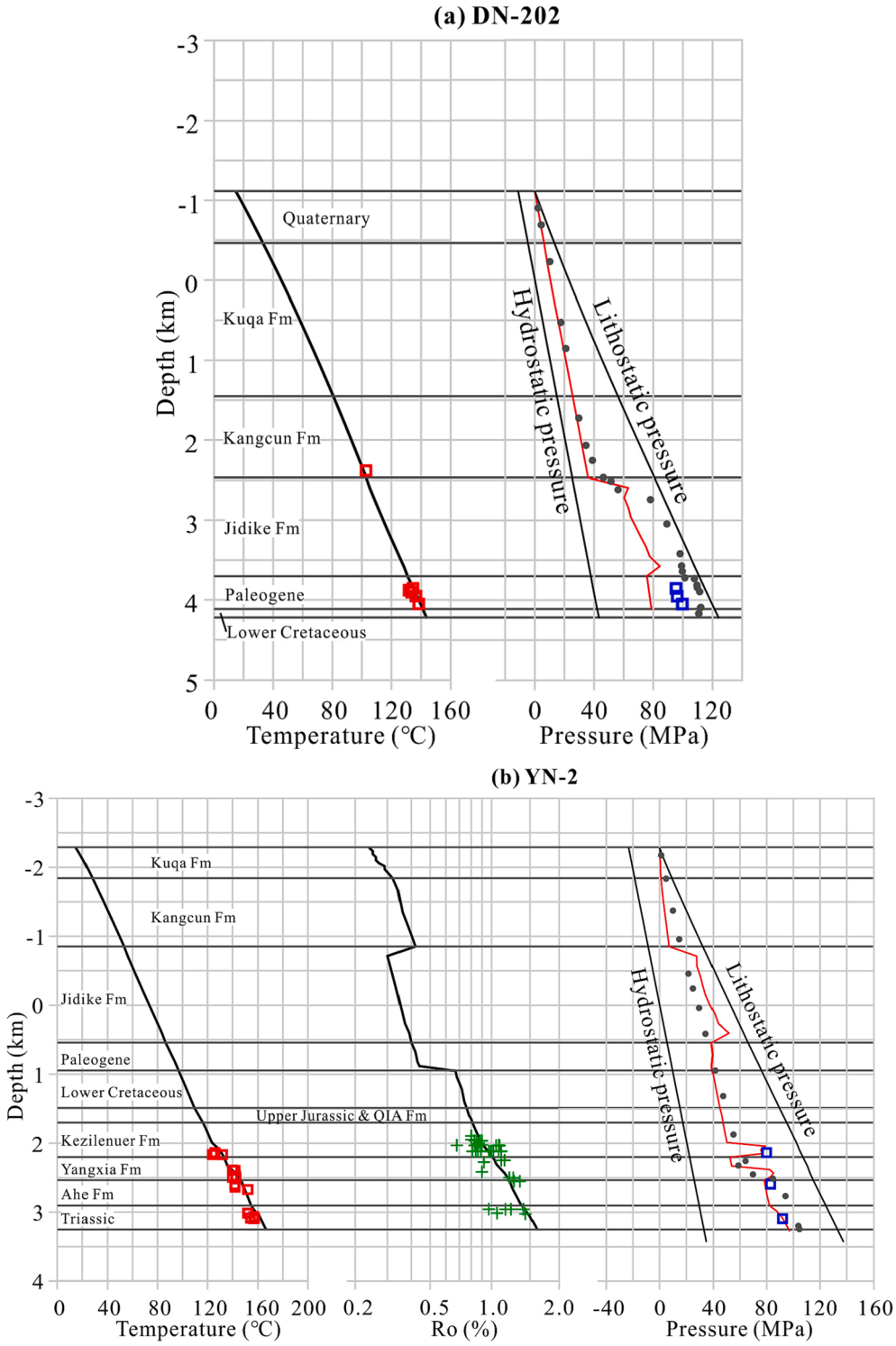

Fig. 9. Plots of modelled values and available calibration data for four wells. Modelled results are extracted from the 2D model (see Fig. 6 for well locations). The measured well temperatures and pressures are from drill stem tests (DSTs). Maturity data include measured ones and converted ones from the Rock-Eval parameter Tmax. mud weights are used as a proxy for pore pressure in the depth interval without the measured pressures. QIA = Qiakemake.

4. Results and discussion

4.1. Model calibration

Key wells DN-202, YN-2, YN-4 and YS-4 were selected for thermal and pressure calibrations (Fig. 9). The measured $\%R_o$ data for each source rock layer are distributed over a wide range. The kinks in the modelled $\%R_o$ trends present in some depth intervals (e.g., the kinks at approximately −1600 m depth in YN-4 and −100 m depth in YS-4) are attributed to the wells drilling through thrust faults. A good calibration was believed to have been achieved and the modelling results are reliable or at least not in conflict with well data when the modelled trends of temperature, $\%R_o$ and pressure were repeatedly adjusted to generate a relatively good match with measurements.

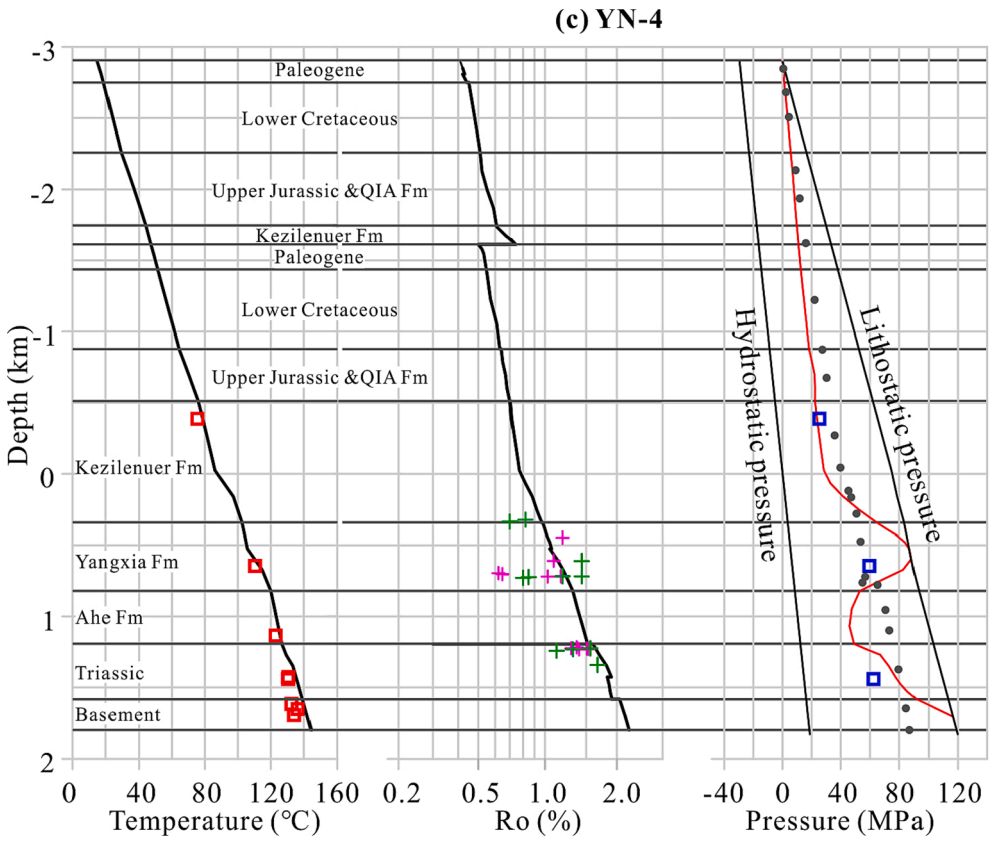

Fig. 9. (*continued*).

4.2. Pressure modelling

The modelling results show that from 23.0 to 16.9 Ma (Fig. 10a, b), overpressures mainly generated in low-permeability intervals of the middle and lower Jurassic and Triassic units, as well as a local overpressure distribution in the Jurassic Kezilenuer Formation. From 5.3 to 2.6 Ma (Fig. 10c, d), the increasing tectonic compression resulted in the development of the Yiqikelike Anticline and Dina Fold Belt. There was a rapid increase in pore pressure on the entire cross-section due to a increased load from both vertical and lateral directions. Basically, overpressure mainly developed within the salt-bearing formation and its underlying units. Overpressure in the Jurassic source rocks was distinctly greater than that of the adjacent reservoir rocks, significantly promoting the primary migration of hydrocarbons. Open faults related to active tectonic activities released overpressure in the rocks near faults. This effect is becoming stronger with increasing rock permeability. Although significant uplift and erosion occur on the northern cross-section at the present day, a combination of continued compressional shortening and the low permeability of the Jidike Formation leads to maximum overpressure within the cross-section (Fig. 10e). The modelled overpressures above the sea level in the northern uplift zone, such as the zone to the north of the fault F9, is due to the groundwater potential associated with elevated topography mentioned previously, which is also suggested in other areas of the Kuqa Depression (Wang et al., 2022). The present-day closed faults are responsible for pressuring compartments showing that there are different overpressures on both sides of a fault.

4.3. Thermal modelling

From 23.0 to 5.3 Ma (Fig. 11a-c), all three layers of source rocks to the south of the fault F8 were in the oil window, indicating both the Jurassic coals and the lacustrine mudstones within the Triassic Taliqike Formation were at the maximum oil generation stage. However, to the north of fault F8, the Taliqike Formation and part of the Jurassic source rocks had entered the wet gas or even dry gas windows reached by relatively high heat flow during the Mesozoic extensional basin stage. At 2.6 Ma (Fig. 11d), the maturation of the source rocks increased due to burial, and the Taliqike and Yangxia formations reached the gas window in the southern part of the section. In contrast, the northern part only showed a slight increase in maturity associated with the increasing folding. At the present day (Fig. 11e), the thermal maturity of source rocks in different areas varies greatly, depending on local tectonic history. For example, continued tectonic subsidence and deposition allow all source rocks in the southern part to reach the gas window. However, most of the source rocks in the Dibei Slope and Yiqikelike Anticline do not have a pronounced maturity increment compared to 2.6 Ma because of the tectonic uplift. At the same depth, there can be different maturity levels on both sides of thrust faults, such as the fault F9.

In the following section, the Yangxia Formation is chosen as an example to show the difference in the evolution of temperature and maturity of source rocks on different structural units. In the Yangxia Sag (Fig. 12a), both temperature and maturity of the source rock show a constant increase during the compression period and have reached a maximum at the present day. Although the Dibei Slope has a similar thermal evolution trend as the Yangxia Sag, except for a brief decline in temperature since 2.6 Ma (Fig. 12b), the present-day thermal regime in the Dibei Slope is much lower due to the smaller subsidence than in the Yangxia Sag. In contrast to the Yangxia Sag and Dibei Slope, the source rocks in the Yiqikelike Anticline reached their maximum temperatures at 100.5 Ma (i.e., prior to the erosion occurring in the Late Cretaceous; Fig. 12c) and witnessed a moderate temperature decline associated with the regional erosion during the Late Cretaceous, followed by a small increase due to the Paleogene deposition. Since the beginning of compression, the constant structural uplift allows source rock to experience an overall decrease in temperature aside from a small increase

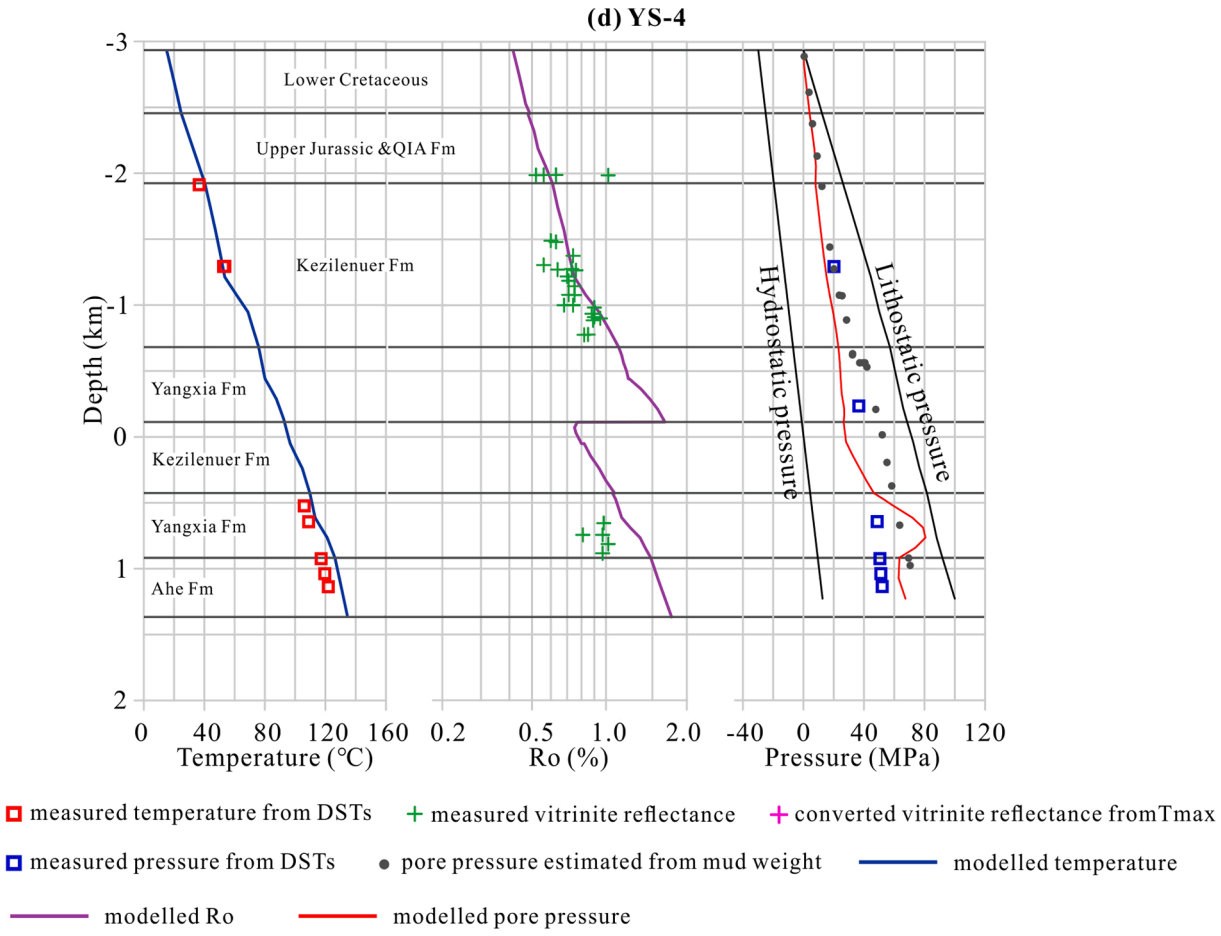

Fig. 9. (*continued*).

from 5.3 to 2.6 Ma caused by the thick Kuqa Formation deposition. Consequently, the maturity has remained almost constant since compression, and the present-day maturity represents the level before tectonic compression.

Although the thermal scenario (i.e., best-fit scenario shown in Fig. 8) used in the model was well calibrated with the measured temperatures and vitrinite reflectance, the paleoheat flow evolution is still highly uncertain. To illustrate the sensitivity of heat flow to the modelled source rocks, an additional high-heat-flow scenario with a constant heat flow of 65 Mw/m^2 (Fig. 8), has been modelled. The modelling results show that the influence of a higher heat flow is closely linked to source rock burial history. For the Yangxia Sag and the Dibei Slope (Fig. 12a, b), the higher heat flow led to a significant increase in the maturity of source rocks after tectonic compression; the deeper the burial, the greater the maturity increase, such as the increment of 0.95 %R_o in the cell A greater than 0.70 %R_o in the cell B. In contrast to the Yangxia Sag and the Dibei Slope, the maturity increase associated with higher heat flow in the Yiqikelike Anticline mainly occurred prior to compression, whereas the maturity difference between the two scenarios has been kept almost constant during compression (Fig. 12c). The modelled results also indicate that the heat flow scenario should be treated more cautiously for petroleum system modelling of tectonically active basins.

4.4. Charge modelling

The petroleum system chart (Fig. 13) summarises the timing of the modelled petroleum system elements and processes in the cross-section, based on a combination of the modelled results and petroleum geologic information. Because the effective charge of hydrocarbons in this study area mainly occurred since the Neogene time (Liang et al., 2003; Pang et al., 2019), the modelled evolution of the petroleum system from 16.9 Ma to the present day is shown in this section.

At 16.9 Ma (Fig. 14a), three paleo structural highs formed and provided good traps for hydrocarbons. The Triassic Taliqike Formation and Jurassic Yangxia Formation showed transformation ratios (TR) of up to 60% and 45%, respectively, whereas the maximum TR of the Jurassic Kezilenuer Formation is below 20%. The generated hydrocarbons were expelled and vertically migrated into the reservoirs in three paleo structural highs. With lateral migration along the tilted reservoirs, the maximum accumulation was modelled in the central structure because of its relatively high altitude. In addition, most oil and gas accumulated in the basal reservoir of the Paleogene seeped to the surface because the caprock did not provide sufficient sealing capacity due to relatively low compaction.

At 5.3 Ma (Fig. 14b), transformation for the Jurassic and Triassic source rocks increased at variable degrees as tectonic compression and depositional loading continued. More hydrocarbons charged the reservoirs of the Ahe, Yangxia, and Kezilenuer formations; sufficient compaction of overlying seal layers allowed hydrocarbons to accumulate at the base of the Paleogene strata. Compared to the previous time step, the Jurassic coals generated a higher proportion of gas due to the increased maturity. The freshly developed faults F8 and F9 extended upward to the surface and caused oil to leak along the faults from deeper parts to the surface; vertical migration along faults also led to the outflow of hydrocarbons within the Yangxia Formation reservoir located to the north of F9.

At 2.6 Ma (Fig. 14c), tectonic compression in the eastern Kuqa Depression continued; the source rock transformation was controlled by local tectonic history. For example, the burial increment caused by both tectonic subsidence and synorogenic deposition increased the TR of

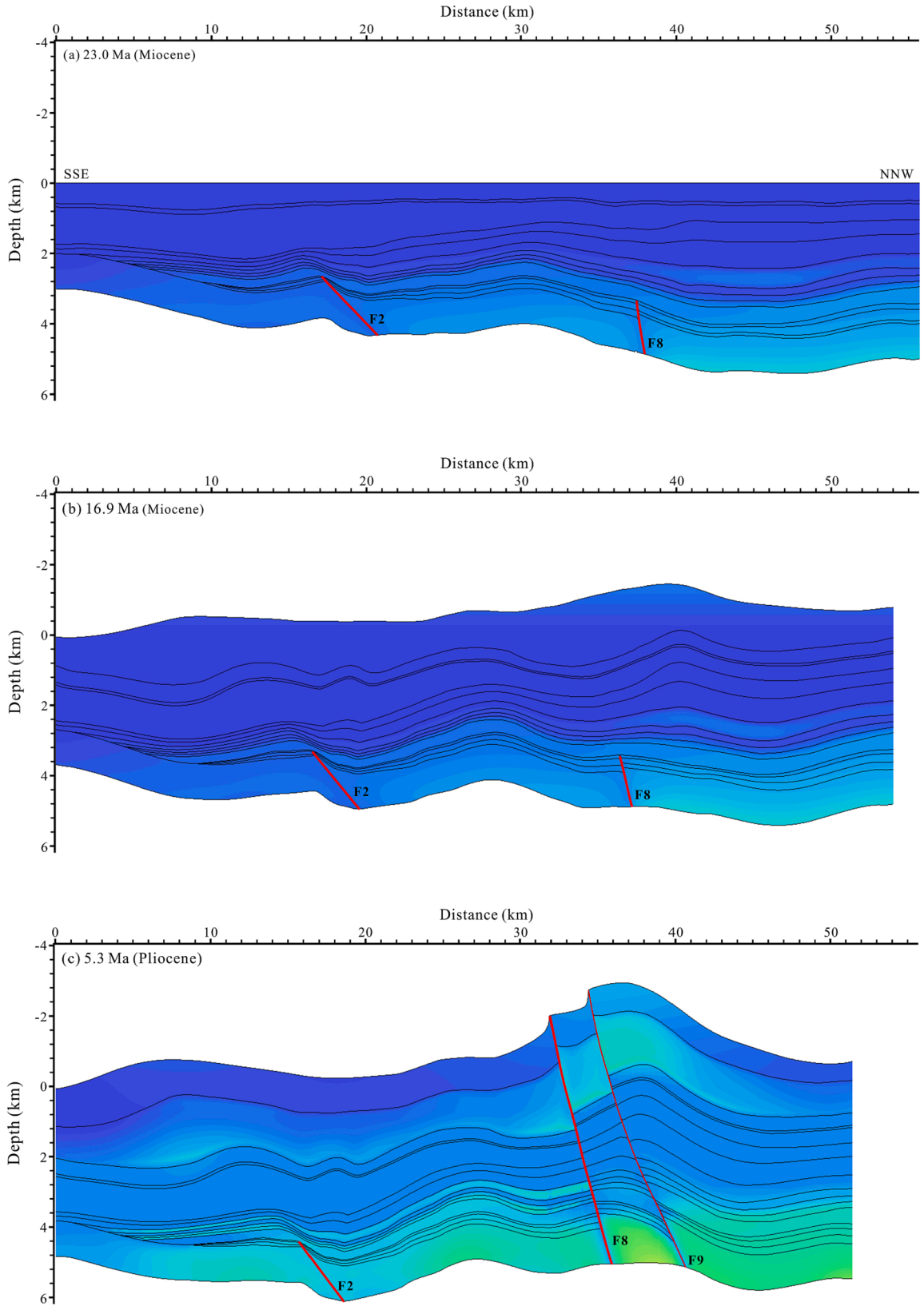

Fig. 10. Development of the modelled overpressure (the pressure difference between pore pressure and hydrostatic pressure) in the basin and petroleum system model by time step.

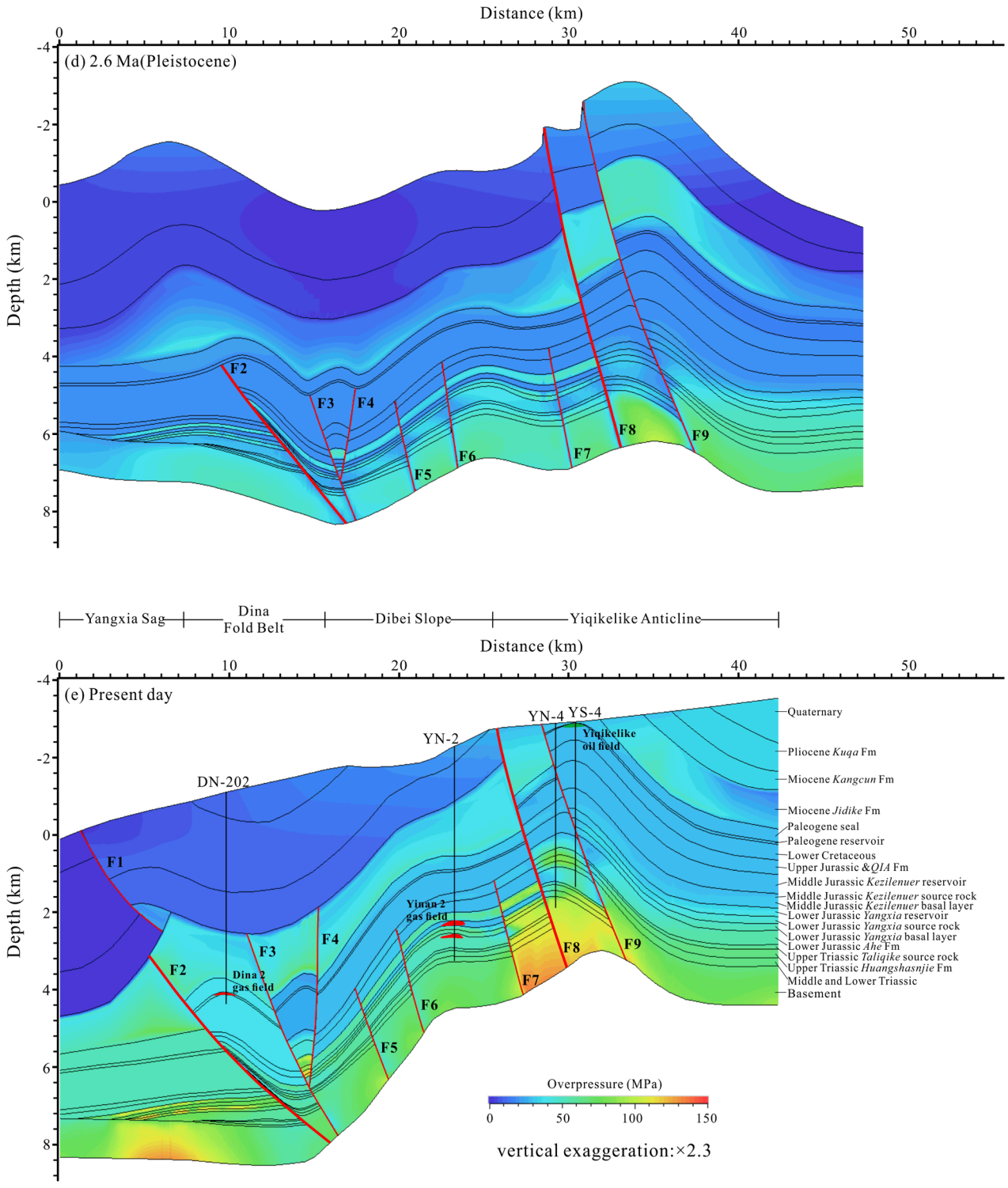

Fig. 10. (*continued*).

source rocks to the south of fault F8, where gas became the dominant type of hydrocarbons. However, source rocks to the north of F8 did not show an increase in TR due to the continued uplift. Because all reverse faults at 2.6 Ma were assumed open, important vertical migration happened along the faults and greatly promoted hydrocarbon charge across different sedimentary units. This is consistent with the previous understanding of fault-controlled migration in the Kuqa Depression (Jia and Li, 2008; Zeng et al., 2010; Zhuo et al., 2014). Consequently, many paleo petroleum systems formed along the cross-section.

At the present day (Fig. 14d), further tectonic compression induces a significant uplift and erosion in the northern section and the more tilted strata of the central section. The prefilled hydrocarbons in reservoirs were adjusted: dissipation or refilling of paleo accumulations occurred. Modelling shows that the Dina2 and Yinan2 gas fields were filled, and they have the reservoirs of the Paleogene strata and the Yangxia Formation, respectively. The present-day accumulations in the Yiqikelike oil field are modelled following an adjustment of the paleo trap during tectonic activities, leaving gas dissipated and residual oil preserved. The

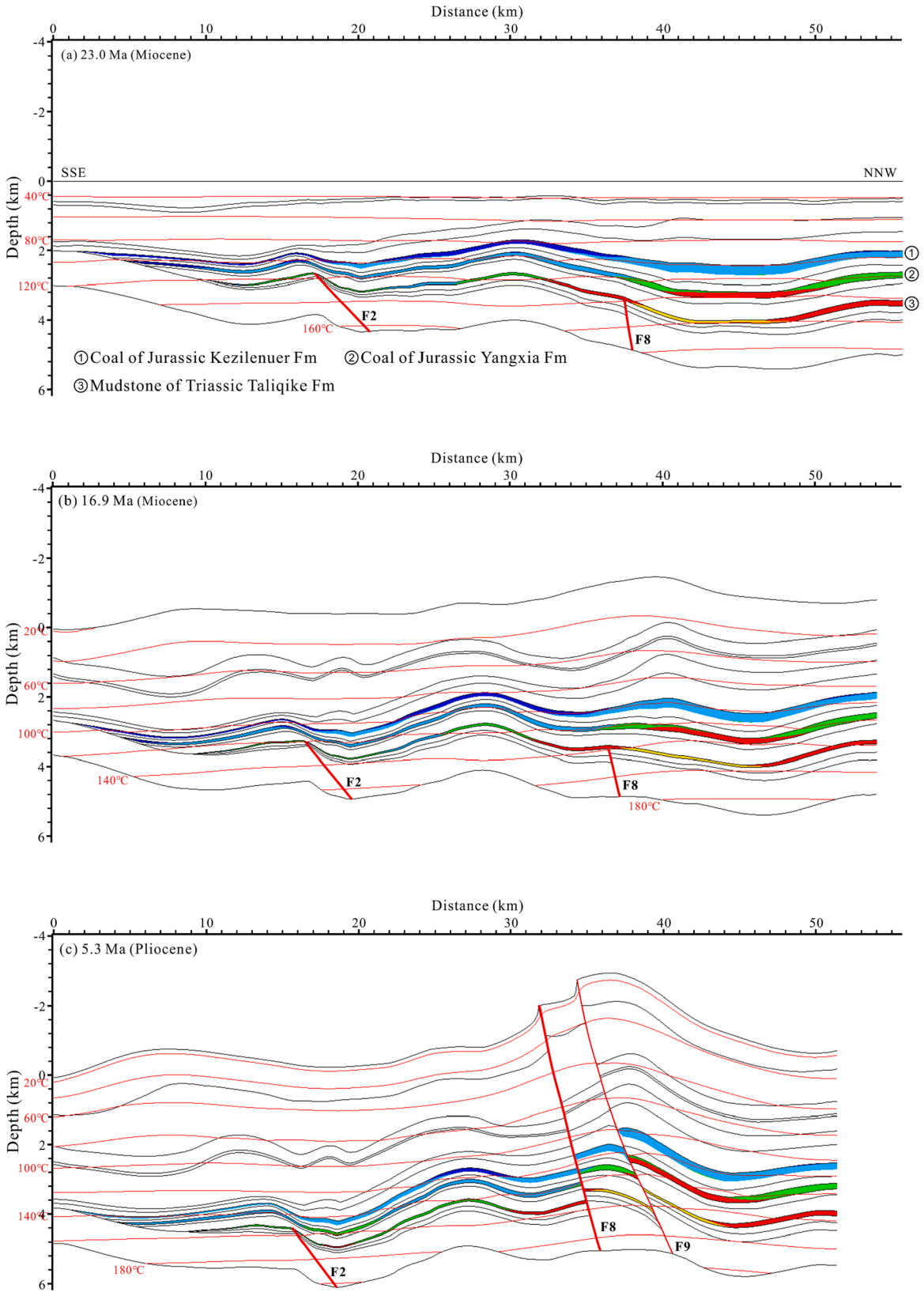

Fig. 11. Evolution map of thermal maturity for coals of the Kezilenuer and Yangxia formations and lacustrine mudstones of the Taliqike Formation, showing the control of tectonic movements on maturity. The thermal maturity was calculated with the Easy%R_o approach of Sweeney & Burnham (1990). (e) Stars represent the extraction locations of cells in Fig. 12.

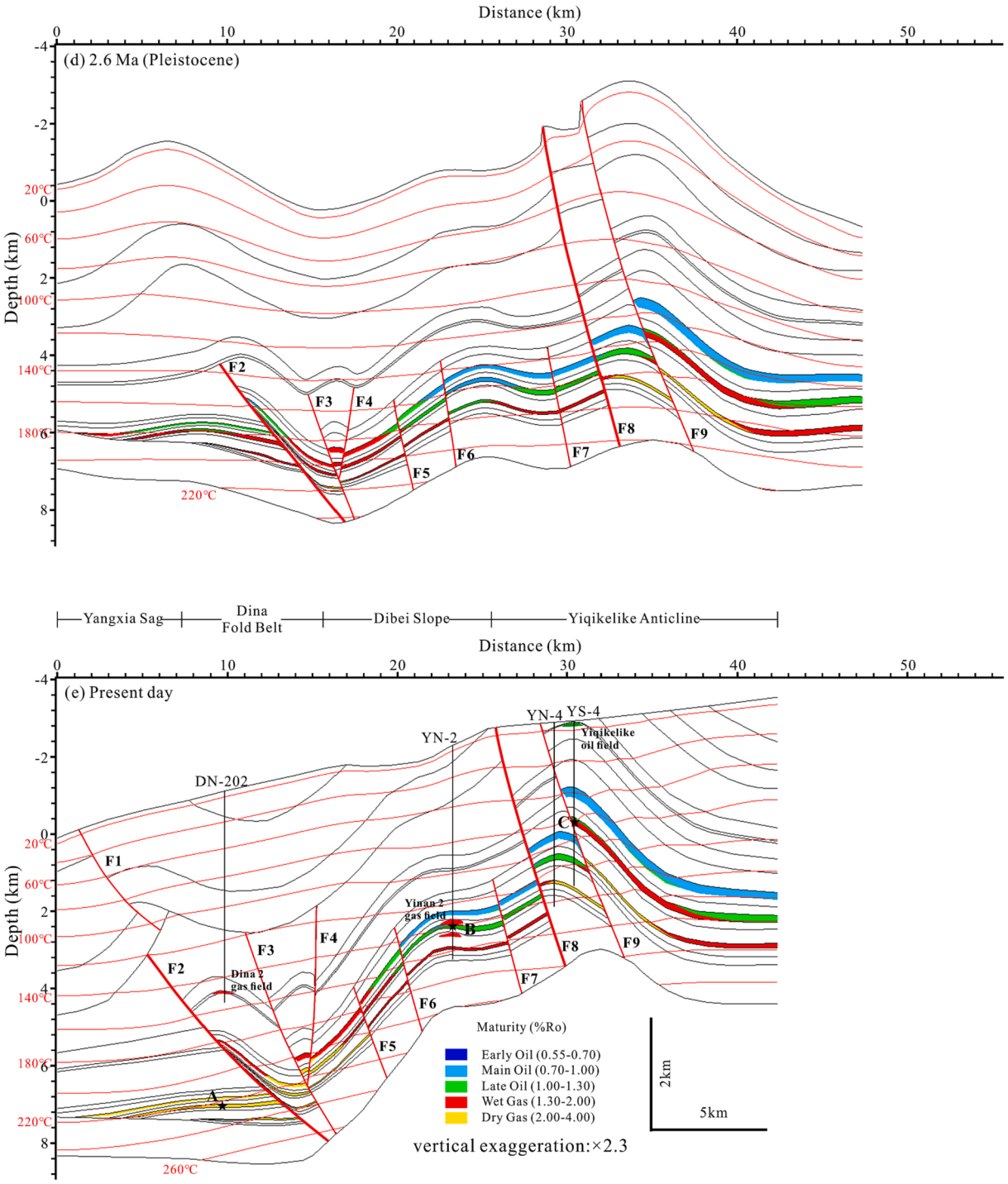

Fig. 11. (*continued*).

modelling also presents an important northward migration along the tilted reservoir layers partly sealed by the closed faults in the Dibei Slope. Even though an important hydrocarbon accumulation in the Jurassic reservoir has been modelled in YN-4 well, the exploration activity suggested only water or a gas–water mixture with a low proportion of gas content for this well (Pang et al., 2019). This discrepancy between the model and reality indicates a high risk of sealing effectiveness in the strong deformed area.

4.5. Hydrocarbon sources

The modelled results suggest that hydrocarbon sources are variable in different fields or even in different reservoirs within a single field (Fig. 15), depending on locally distinct basin histories. Hydrocarbons in the Ahe Formation of the Yinan2 gas field originate from both the Taliqike Formation mudstones and the Yangxia Formation coals, those in the reservoir within the Yangxia Formation from the Yangxia Formation coals, and those in the Kezilenuer Formation reservoir from a mixture of the Yangxia and Kezilenuer formations coals. For the reservoir at the base of the Paleogene in the Dina2 gas field and the shallow reservoir in the Yiqikelike oil field, the hydrocarbons were generated from the Yangxia and Kezilenuer formations coaly source rocks. The modelled results are in good agreement with previous conclusions obtained by biomarker, stable carbon isotope and fluid inclusions analyses

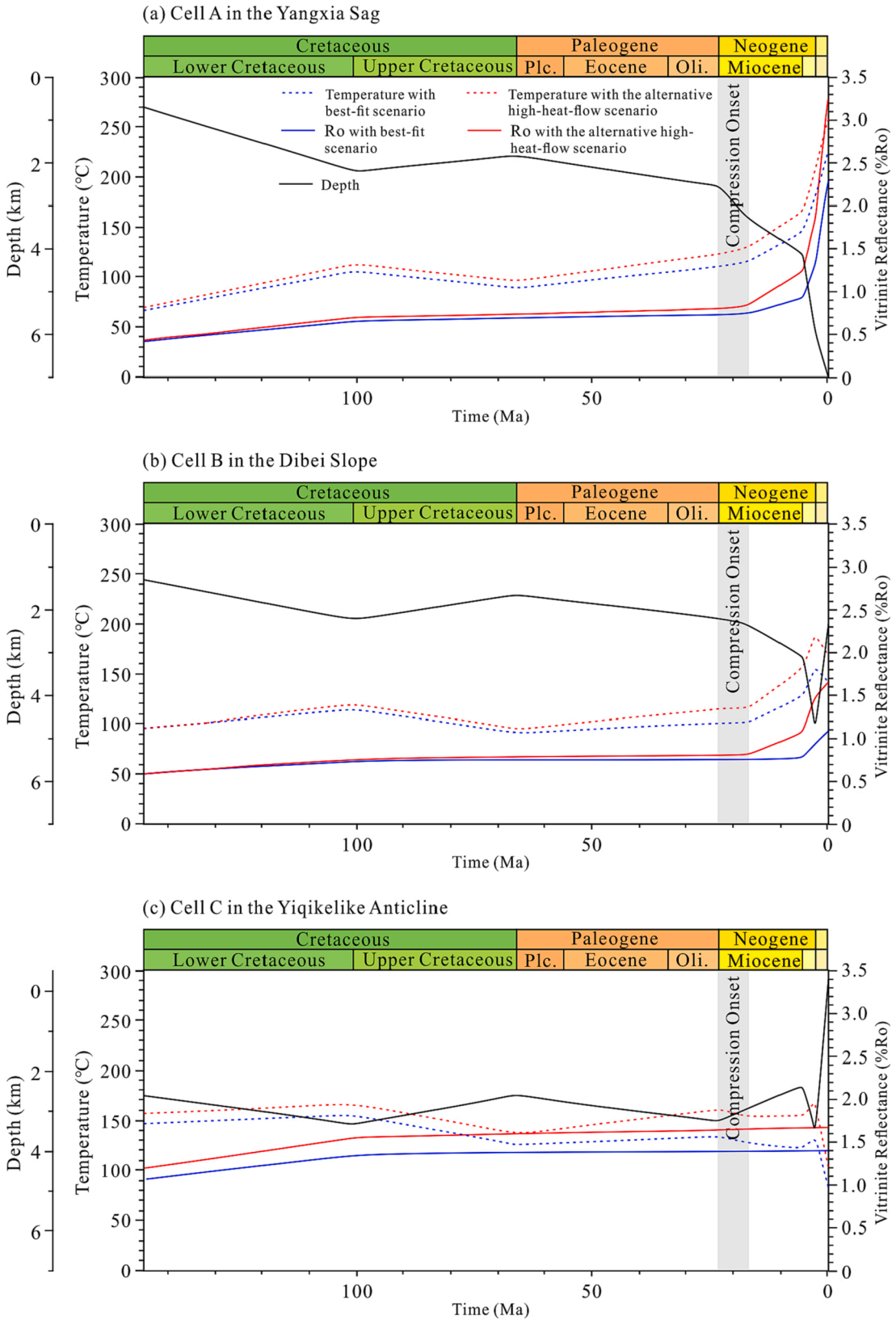

Fig. 12. Temperature and thermal maturity through time for the Yangxia Formation source rocks in different structural units (extraction locations in Fig. 11e), showing the heat flow sensitivity to the source rocks.

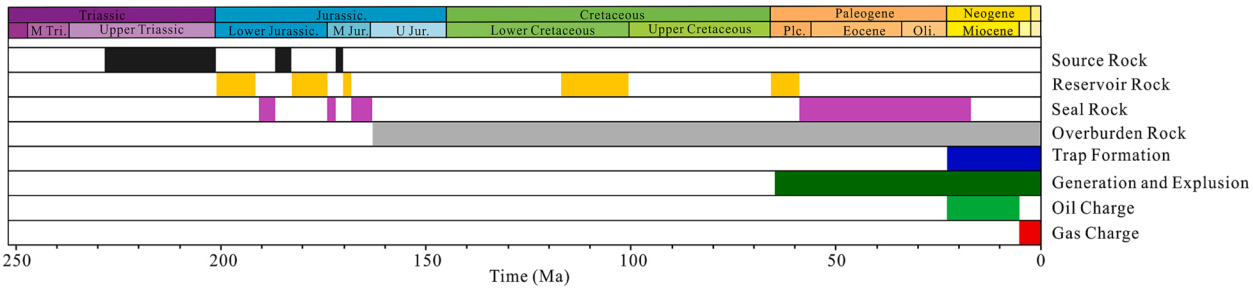

Fig. 13. Petroleum system events chart based on the modelled results and the knowledge of petroleum geologic setting in the study area.

(Ni et al., 2013; Fan et al., 2014; Song et al., 2019).

Additionally, previous studies suggested two episodes of hydrocarbon charge: an early oil charge in the Miocene and late gas charge from the Pliocene onward (Liang et al., 2003; Pang et al., 2019). However, our model suggests that even at the stage of low maturity of the Jurassic coal seams, high amounts of natural gas with some accompanied oil were generated (Fig. 14a). In fact, for a coaly source rock, the generation of hydrocarbon gas typically appears to be accompanied by a certain amount of light oil during early thermal evolution. (Littke and Leythaeuser, 1993).

4.6. Prospectivity

We modelled the charge of the main fields, including the Dina2, Yinan2 gas fields, and the Yiqikelike oil field. Other prospects were analysed as well. An important lateral migration is modelled along the tilted carrier beds, which are sealed by the closed faults in the Dibei Slope. Hydrocarbon accumulations mainly occur in the Ahe, Yangxia and Kezilenuer reservoir layers. Additionally, some accumulations related to faults are also developed in the Dina Fold Belt. Therefore, the fault-related traps in the Dibei Slope and the Dina Fold Belt should be considered by petroleum geologists in the future. A Tight sandstone reservoir is defined as a sandstone reservoir with low porosity and permeability (Masters, 1979). There is no defined uniform standard regarding reservoir properties for tight sandstone reservoirs worldwide. “Geological evaluating methods for tight sandstone gas (SY/T 6832-2011)” issued by the National Energy Administration of China, suggests tight sandstone reservoirs to have less than 10% porosity and a permeability of less than 1mD at ambient laboratory conditions. Tight gas accumulations are characterised by continuously distributed gas-bearing sandstone bodies, no distinct trap boundary, complex gas–-water relationships (a typical example of inverted gas–water), and buoyancy having only minor effects on migration (Pang et al., 2019). The experiments on a large number of core samples from the Jurassic reservoirs in the study area show that porosity of the most samples ranges from 1% to 12%; permeability ranges from 0.01 to 356.8 mD, where about 85% of total samples have permeability lower than 1 mD (Jiang et al., 2016; Pang et al., 2019; Zhao et al., 2022). Additionally, an “inverted gas–water relationship” has been extensively observed (Wang et al., 2018): within a single reservoir unit, water is present in an updip structural position, while gas filled occurs in a downdip structural position. This type of inverted relationship is mainly due to the strong tightness of the reservoir preventing upward migration. The above data observed indicate the presence of tight sandstone reservoirs with in the Jurassic units in the study area. Combined with high-maturity coals as the important gas sources, the area should be treated as a good candidate for tight sandstone gas.

In the study area, rock failure related to stress and differential diagenesis are critical risks indicated by the disagreement between modelling results and drilling discoveries such as the YN-4 well. This difference may be explained by the following two factors: (1) Given the compressional tectonics in the study area, a poro-elastic approach has been applied in the model to consider the relationship between stress, pore pressure and strain. However, the poro-elastic approach is unable to account for rock plastic deformation (e.g., shear failure) related to deviator stress. As a result, no shear failure of rock occurs where stresses exceed the failure criterion, which means hydrocarbon dissipation cannot be modelled. In reality, shear fractures have been observed in some cores in the Yiqikelike Anticline (Jiang et al., 2015; Lu et al., 2016), which cannot be modelled due to the limitations stated above. (2) As mentioned previously, this model is unable to account for differential diagenesis and the resulting heterogeneity in petrophysical properties (e.g., porosity and permeability). Heterogeneous reservoirs have been indicated by microscopic observation of rock samples and complicated gas–water relationship (Guo et al., 2018; Zhang et al., 2021) in the study area, and may influence the migration and accumulation of hydrocarbons. Besides, highly mature source rocks with fractures are typically considered good shale gas reservoirs (Curtis, 2002). Therefore, the fractured Triassic source rock around the Yiqikelike Anticline likely acts as a potentially favourable zone for shale gas.

4.7. Limitation and uncertainty analysis

Because the petroleum system model is a conceptual model based on the geological evolution of a basin rather than a “copy” of the real basin, there inevitably exist some simplifications, limitations, or uncertainties in the conceptual model (Brandes et al., 2008). For example, even though the mixed lithologies and an average TOC content were assigned for each source rock layer in the model, the realistic volume of potential source rock and TOC and HI are likely variable at different locations, which may have a certain impact on hydrocarbon charge modelling. Unfortunately, simplifications had to be made due to limited data for modelling. Furthermore, a laterally consistent lithology in each stratigraphic layer was assumed for simplification. The cross-section, however, is likely more complex, especially for the reservoirs, where laterally variable facies or differential chemical diagenesis caused a significant heterogeneity in permeabilities, further altering the migration and accumulation conditions. Additionally, all hydrocarbon accumulations form through the migration only in the direction of the modelled 2D section rather than in three dimensions.

In addition, as mentioned previously, a simplified fracture model based on the Griffith theory was used in this simulation in which fracturing occurs when pore pressure exceeds the defined fracture pressure. More advanced plastic deformation was not considered, and consequently, rock failure due to stress is not addressed well. In particular, rock failure in deeper units or complex deformation zones might be less accurately modelled, which could influence simulation results of expulsion, migration and preservation of hydrocarbons.

The present-day and reconstructed paleo-geometries are treated as input parameters for numerical simulation and significantly influence the quality of petroleum system modelling, including thermal maturity, pressures, and charge. However, two main factors usually cause some uncertainties in the basin geometry: (1) There are uncertainties in the interpretation of stratigraphic horizons and faults based on the seismic

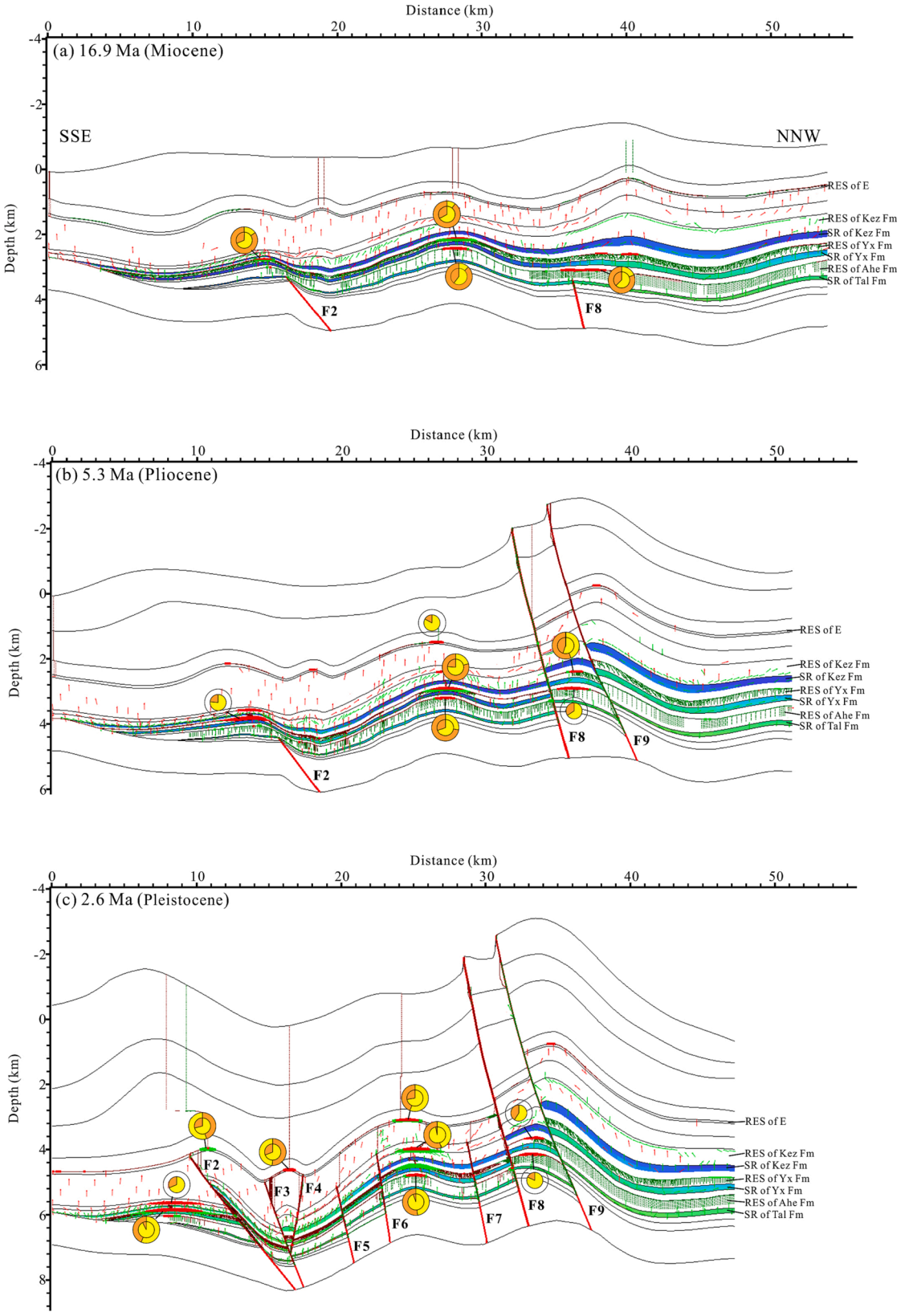

Fig. 14. Migration and accumulation of hydrocarbons with modelled transformation ratio for source rock layers. Darcy (arrow) and Invasion Percolation (curve) algorithms were used to model hydrocarbon migration. Along the migration pathways and in the accumulation, red and green colours represent hydrocarbons in the vapour and liquid phases, respectively. The pie charts show the relative proportion of oil (orange colour) and gas (yellow colour) components and phase state in situ for hydrocarbon accumulations, where the inner and outer circles represent vapour and liquid phases, respectively. RES = reservoir, SR = source rock, Kez = Kezilenuer, Yx = Yangxia, Tal = Taliqike. (For interpretation of the references to colour in this figure legend, the reader is referred to the web version of this article.)

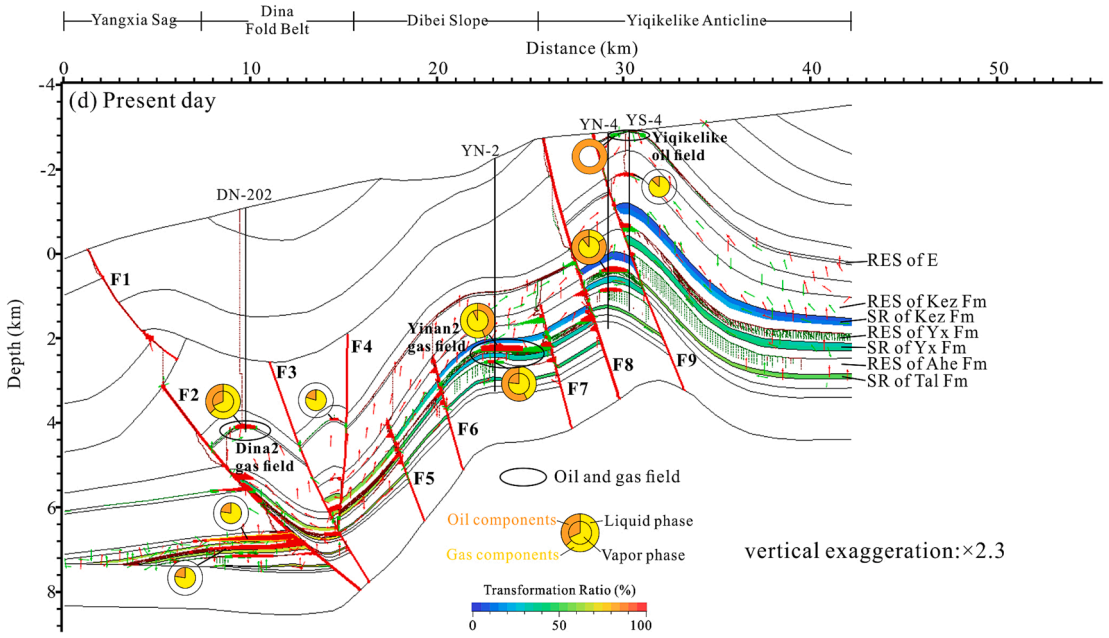

Fig. 14. (*continued*).

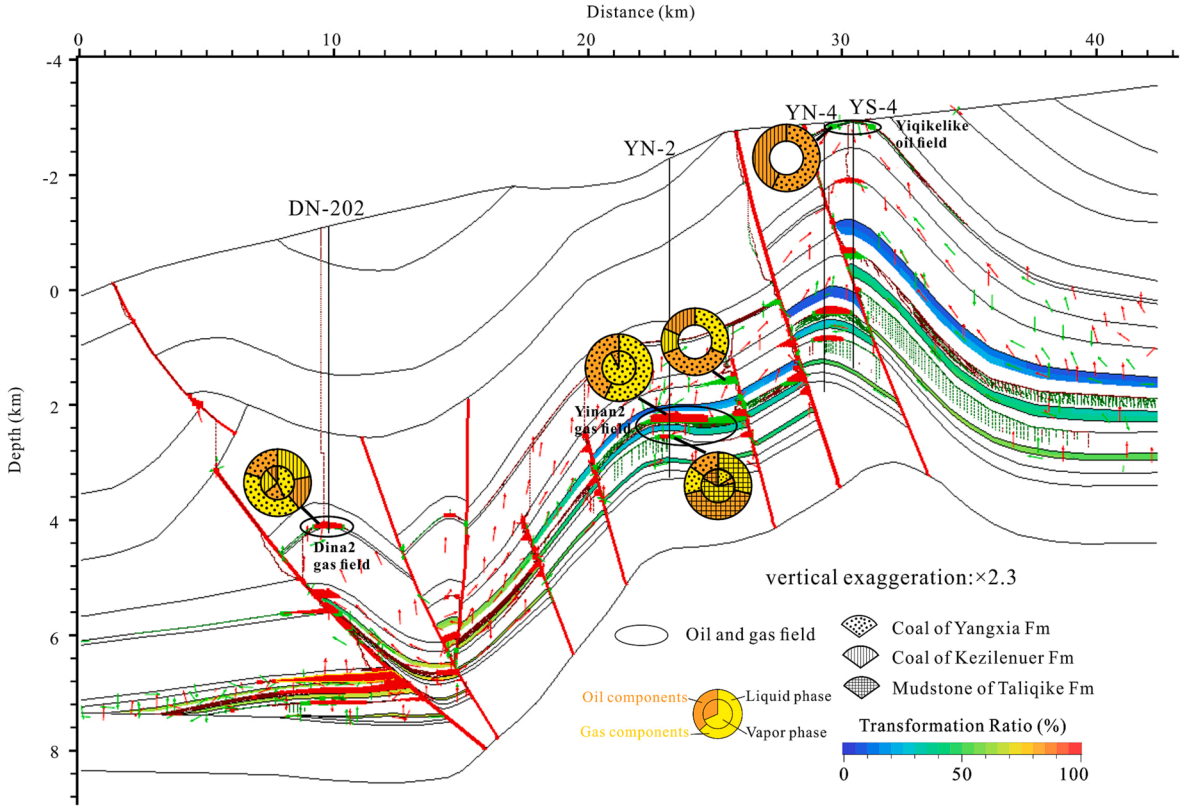

Fig. 15. Hydrocarbon sources of accumulations at the present day. The pie charts show the relative proportion of oil (orange colour) and gas (yellow colour) components and phase state in situ for hydrocarbon accumulations, where the inner and outer circles represent vapour and liquid phases, respectively, and filled patterns in slices represent different sources of hydrocarbons. (For interpretation of the references to colour in this figure legend, the reader is referred to the web version of this article.)

section with poor local quality, and (2) the structural reconstruction may induce additional structural uncertainties. For example, the incremental displacements of faults at each time step are poorly constrained, although the fault evolution in the structural reconstruction is generally consistent with the knowledge of the regional tectonic development.

5. Conclusions

(1) This study highlights the need for a structural model to reconstruct the development of a petroleum system in a compressional tectonic setting and shows how the structural evolution controls the

thermal evolution of source rocks and hydrocarbon charge.

(2) Distinct local structural histories appear to impact the maturity of source rocks significantly. Prior to tectonic compression, the northern part of the area was thermally more mature than the central and southern parts due to greater burial. Since the beginning of compression, the southern and central parts of the area have been experiencing a continuous increase in maturity due to structural subsidence, whereas a uplift causes the maturity level in the northern part to remain unchanged.

(3) The present-day hydrocarbon accumulations are the combined results of multiple stages of charges and late structural adjustment. The proportion of gases was increasing with increasing maturity of Jurassic and Triassic source rocks. Modelled hydrocarbon accumulations occur mainly in the Dina Fold Belt and the Dibei Slope, with key reservoirs in the Ahe, Yangxia and Kezilenuer formations in the Jurassic and at the base of the Paleogene.

(4) The different sources of hydrocarbons in various reservoirs are recognised, indicating mixed source characteristics. Besides, the fold- and fault-related traps and tight sandstone reservoirs in the Dina Fold Belt and the Dibei Slope are considered favourable exploration targets.

CRediT authorship contribution statement

Bing Wang: Conceptualization, Data curation, Formal analysis, Methodology, Writing – original draft. **Nansheng Qiu:** Supervision, Project administration, Funding acquisition. **Ralf Littke:** Supervision, Writing – review & editing. **Sebastian Amberg:** Formal analysis, Writing – review & editing. **Zhengdong Liu:** Resources.

Declaration of Competing Interest

The authors declare that they have no known competing financial interests or personal relationships that could have appeared to influence the work reported in this paper.

Data availability

Data will be made available on request.

Acknowledgements

This study is financially funded by the National Nature Science Foundation of China (Grant No. U19B6003) and the Science and Technology Project from PetroChina Tarim Oilfield Company (Grant No. 041020050021). PetroChina Tarim Oilfield Company is thanked for providing seismic and well data. Finally we thank Gabor Tari, the anonymous reviewers and associate editor Ahmed Radwan for their constructive comments which helped to improve the manuscript.

References

Al-Hajeri, M.M., Saeed, A.M., Derks, J., Fuchs, T., Hantschel, T., Kauerauf, A., Neumaier, M., Schenk, O., Swientek, O., Tessen, N., Welte, D., Wygrala, B., 2009. Basin and petroleum system modeling. Oilfield Rev. 21, 14–29.

Allen, M.B., Vincent, S.J., Wheeler, P.J., 1999. Late Cenozoic tectonics of the Kepingtage thrust zone: interactions of the Tien Shan and Tarim Basin, northwest China. Tectonics 18, 639–654.

Baur, F., Benedetto, M.D., Fuchs, T., Lampe, C., Sciamanna, S., 2009. Integrating structural geology and petroleum systems modeling–A pilot project from Bolivia's fold and thrust belt. Mar. Pet. Geol. 26, 573–579.

Baur, F., Di Primio, R., Lampe, C., Littke, R., 2011. Mass balance calculations for different models of hydrocarbon migration in the Jeanne d'Arc basins, offshore Newfoundland. J. Pet. Geol 34, 181–198.

Baur, F., Katz, B., 2018. Some practical guidance for petroleum migration modeling. Mar. Pet. Geol. 93, 409–421.

Brandes, C., Astorga, A., Littke, R., Winsemann, J., 2008. Basin modelling of the Limón Back-arc Basin (Costa Rica): burial history and temperature evolution of an island arc-related basin-system. Basin Res. 20, 119–142.

Burgreen-Chan, B., Graham, S.A., 2018. Petroleum system modeling of the East Coast Basin, Hawke Bay, New Zealand. AAPG Bull. 102, 587–612.

Burgreen-Chan, B., Meisling, K.E., Graham, S., 2016. Basin and petroleum system modelling of the East Coast Basin, New Zealand: a test of overpressure scenarios in a convergent margin. Basin Res. 28, 536–567.

Burnham, A.K., 1989. A simple kinetic model of petroleum formation and cracking. Lawrence Livermore Lab. Report UCID 21665, March.

Curtis, J.B., 2002. Fractured shale-gas systems. AAPG Bull. 86, 1921–1938.

D'Ambrosio, A., Lipparini, L., Bigi, S., Cassola, T., Bambridge, V.R., Derks, J.F., Trippetta, F., 2021. Structural restoration and basin modelling of the central apennine orogen/foredeep/foreland system: New insights on the regional petroleum system. Mar. Pet. Geol. 127, 104948.

England, W.A., Mackenzie, A.S., Mann, D.M., Quigley, T.M., 1987. The movement and entrapment of petroleum fluids in the subsurface. J. Geol. Soc. London 144, 327–347.

Fan, J.J., Pan, M., Zhou, H.M., Liu, S.B., Zhuo, Q.G., Zheng, Y.P., 2014. Hydrocarbon migration pathway and charging characterisation of Yinan-2 gas reservoir in Kuqa Depression. Acta Sci. Nat. Univ. Pekin. 50, 507–514 in Chinese with English abstract.

Förster, A., Merriam, D.F., Davis, J.C., 1997. Spatial analysis of temperature (BHT/DST) data and consequences for heat-flow determination in sedimentary basins. Geol. Rundsch. 86, 252–261.

Froidl, F., Zieger, L., Mahlstedt, N., Littke, R., 2020. Comparison of single- and multi-ramp bulk kinetics for a natural maturity series of Westphalian coals: Implications for modelling petroleum generation. Int. J. Coal Geol. 219, 103378.

Fu, X.F., Jia, R., Wang, H.X., Wu, T., Meng, L.D., Sun, Y.H., 2015. Quantitative evaluation of fault-caprock sealing capacity: A case from Dabei-Kelasu structural belt in Kuqa Depression, Tarim Basin, NW China. Pet. Explor. Dev. 42, 329–338.

Graham, S.A., Hendrix, M.S., Wang, L.B., Homewood, P., 1993. Collision successor basins of western China, impact of tectonic inheritance on sand composition. Geol. Soc. Am. Bull. 105, 323–344.

Guo, S., Lyu, X.X., Zhang, Y., 2018. Relationship between tight sandstone reservoir formation and hydrocarbon charging: A case study of a Jurassic reservoir in the eastern Kuqa Depression, Tarim Basin, NW China. J. Nat. Gas Sci. Eng. 52, 304–316.

Guo, X.W., Liu, K.Y., Jia, C.Z., Song, Y., Zhao, M.J., Lu, X.S., 2016. Effects of early petroleum charge and overpressure on reservoir porosity preservation in the giant Kela-2 gas field, Kuqa depression, Tarim Basin, northwest China. AAPG Bull. 100, 191–212.

Hantschel, T., Kauerauf, A.I., 2009. Fundamentals of Basin and Petroleum Systems Modeling. Springer, Berlin.

Huang, W.K., Zeng, L.F., Pan, C.C., Xiao, Z.Y., Zhang, H.Z., Huang, Z.B., Zhao, Q., Yu, S., Xu, H., Chen, C.S., Liu, D.Y., Jiu, J.Z., 2019. Petroleum generation potentials and kinetics of coaly source rocks in the Kuqa Depression of Tarim Basin, northwest China. Org Geochem. 133, 32–52.

Jarvie, D.M., Lundell, L.L., 2001. Kerogen type and thermal transformation of organic matter in the Miocene Monterey Formation. In: Isaacs, C.M., Rullkötter, J. (Eds.), The Monterey Formation-from Rocks to Molecules. Columbia University Press, New York.

Jia, C.Z., Li, Q.M., 2008. Petroleum geology of Kela-2, the most productive gas field in China. Mar. Pet. Geol. 25, 335–343.

Jiang, F.J., Pang, X.Q., Guo, F.T., Guo, J.G., 2016. Critical conditions for natural gas charging and delineation of effective gas source rocks for tight sandstone reservoirs. Geol. J. 51, 113–124.

Jiang, Z.X., Li, F., Yang, H.J., Li, Z., Liu, L.F., Chen, L., Du, Z.M., 2015. Development characteristics of fractures in Jurassic tight reservoir in Dibei area of Kuqa depression and its reservoir-controlling mode. Acta Pet. Sin. 36, 102–111.

King, R.C., Backé, G., Morley, C.K., Hillis, R.R., Tingay, M.R.P., 2010. Balancing deformation in NW Borneo: Quantifying plate-scale vs. gravitational tectonics in a delta and deepwater fold-thrust belt system. Mar. Pet. Geol. 27, 238–246.

Li, F., Jiang, J.X., Li, Z., Xiao, Z.Y., Yuan, W.F., Cao, S.Y., Du, Z.M., 2014. Paleo-fluid evidence for the two-stage hydrocarbon charges in Dibei gas reservoir of Kuqa Depression. Nat. Gas Geosci. 25, 1033–1041 in Chinese with English abstract.

Li, X.Q., Xiao, X., Mi, J.K., Tang, Y.C., Xiao, Z.Y., Liu, D., Shen, J.G., Yang, Y.F., Wang, Y., Dong, P., 2008. Kinetic Parameters of Methane Generated from Source Rocks in the Kuqa Depression of Tarim Basin and Their Application. Acta Geol. Sin. 82, 154–163.

Li, M.J., Wang, T.G., Chen, J.F., He, F.Q., Yun, L., Akbar, S., Zhang, W.B., 2010. Paleo-heat flow evolution of the Tabei Uplift in Tarim Basin, northwest China. J. Asian Earth Sci. 37, 52–66.

Li, S.Q., Wang, X., Suppe, J., 2012. Compressional salt tectonics and synkinematic strata of the western Kuqa foreland basin, southern Tian Shan, China. Basin Res. 24, 475–497.

Li, Z., Wang, Q.C., Wang, D.X., Lin, W., 2003. Depositional record constraints on Late Cenozoic uplift of Tianshan and tectonic transformation in Kuqa Depression, west China. Acta Sedimentological Sinica 21, 38–45.

Liang, D.G., Zhang, S.C., Chen, J.P., Wang, F.Y., Wang, P.R., 2003. Organic geochemistry of oil and gas in the Kuqa depression, Tarim Basin, NW China. Org Geochem. 34, 873–888.

Lipparini, L., D'Ambrosio, A., Trippetta, F., Bigi, S., Derks, J.F., Bambridge, V.R., Cassola, T., 2021. A new regional petroleum systems model for central italy and the central adriatic sea supported by basin modelling and an analysis of hydrocarbon occurrences. J. Pet. Geol 44, 461–485.

Littke, R., Leythaeuser, D., 1993. Migration of oil and gas in coals. AAPG Bull. 38, 219–236.

Liu, Q.Y., Zhang, T.W., Jin, Z.J., Qin, S.F., Tang, Y.C., Liu, W.H., 2011. Kinetic Model of Gaseous Alkanes Formed from Coal in a Confined System and Its Application to Gas Filling History in Kuqa Depression, Tarim Basin, Northwest China. Acta Geol. Sin. 85, 911–922.

Liu, R.H., Li, J., Xiao, Z.Y., Li, J., Zhang, H.Z., Lu, Y.H., Zhang, B.S., Ma, W., Li, D.J., Liu, M.C., 2019. Geochemical characteristics and their gas and oil source correlation

implication in the Tugeerming area of the Kuqa Depression, Tarim Basin, China. J. Nat. Gas Geosci. 4, 161–168.
Lu, H., Lu, X.S., Fan, J.J., Zhao, M.J., Wei, H.X., Zhang, B.S., Lu, Y.H., 2016. Controlling effect of fractures on gas accumulation and production within the tight sandstone: A case study on the Jurassic Dibei gas reservoir in the eastern part of the Kuqa foreland basin, China. J. Nat. Gas Geosci. 1, 61–71.
Lu, H. F., Jia, D., Chen, C. M., Cai, D. S., Wu, S. M., Wang, G. Q., Guo, L. Z., Shi, Y. S., 1997. Evidence for growth fault-bent folds in the Tarim Basin and its implications for fault-slip rates in theMesozoic and Cenozoic. In: Structural geology and geomechanics (Ed. by Zheng, Y.D., Davis, G.A. & Yin, A.). Proceedings of the 30th International Geological Congress. IUGS, Boca Raton, Florida.
Maerten, L., Maerten, F., 2006. Chronologic modeling of faulted and fractured reservoirs using geomechanically based restoration: Technique and industry applications. AAPG Bull. 90, 1201–1226.
Masters, J.A., 1979. Deep basin gas trap, western Canada. AAPG Bull. 63, 152–181.
Matte, P.H., Tapponnier, P., Arnaud, N., Bourjot, L., Avouac, J.P., Vidal, P., Liu, Q., Pan, Y.S., Wang, Y., 1996. Tectonics of Western Tibet, between the Tarim and the Indus. Earth Planet. Sci. Lett. 142, 311–330.
Neumaier, M., Littke, R., Hantschel, T., Maerten, L., Joonnekindt, J.P., Kukla, P., 2014. Integrated charge and seal assessment in the Monagas fold and thrust belt of Venezuela. AAPG Bull. 98, 1325–1350.
Ni, Y.Y., Dai, J.X., Zhu, G.Y., Zhang, S.C., Zhang, D.J., Su, J., Tao, X.W., Liao, F.R., Wu, W., Gong, D.Y., Liu, Q.Y., 2013. Stable hydrogen and carbon isotopic ratios of coal-derived and oil-derived gases: A case study in the Tarim basin, NW China. Int. J. Coal Geol. 116–117, 302–313.
Pang, X.Q., Peng, J.W., Jiang, Z.X., Yang, H.J., Wang, P.W., Jiang, F.J., Wang, K., 2019. Hydrocarbon accumulation processes and mechanisms in Lower Jurassic tight sandstone reservoirs in the Kuqa subbasin, Tarim Basin, northwest China: A case study of the Dibei tight gas field. AAPG Bull. 103, 769–796.
Qin, S.F., Dai, J.X., Liu, X.W., 2007. The controlling factors of oil and gas generation from coal in the Kuqa Depression of Tarim Basin, China. Int. J. Coal Geol. 70, 255–263.
Qiu, N.S., Chang, J., Li, J.W., Li, W.Z., Yun, L., Li, H.L., 2012. New evidence on the Neogene uplift of South Tianshan: constraints from the (U–Th)/He and AFT ages of borehole samples of the Tarim basin and implications for hydrocarbon generation. Int. J. Earth Sci. 101, 1625–1643.
Song, X., Lv, X.X., Shen, Y.Q., Guo, S., 2019. Hydrocarbon migration and accumulation history in deep reservoirs: a case study of Mesozoic sandstone gas reservoirs in the Kelasu-Yiqikelike structural belt of the Kuqa Depression, Tarim Basin. Geosci. J. 23, 69–86.
Sweeney, J.J., Burnham, A.K., 1990. Evaluation of a simple model of vitrinite reflectance based on chemical kinetics. AAPG Bull. 74, 1559–1570.
Tang, L.J., Jia, C.Z., Jin, Z.J., Chen, S.P., Pi, X.J., Xie, H.W., 2004. Salt tectonic evolution and hydrocarbon accumulation of Kuqa foreland fold belt, Tarim Basin, NW China. J. Pet. Sci. Eng. 41, 97–108.
Tang, X.Y., Yang, S.C., Hu, S.B., 2014. Thermal and Maturation History of Jurassic Source Rocks in the Kuqa Foreland Depression of Tarim Basin, NW China. J. Asian Earth Sci. 89, 1–9.
Wang, B., Qiu, N., Amberg, S., Duan, Y., Littke, R., 2022. Modelling of pore pressure evolution in a compressional tectonic setting: the Kuqa Depression, Tarim Basin, northwestern China. Mar. Pet. Geol. 146, 105936.
Wan, J.L., Gong, Y.J., Huang, W.H., Zhuo, Q.G., Lu, X.S., 2022. Characteristics of hydrocarbon migration and accumulation in the Lower Jurassic reservoirs in the Tugerming area of the eastern Kuqa Depression, Tarim Basin. J. Pet. Sci. Eng. 208, 109748.
Wang, L.S., Li, C., Liu, S.W., Li, H., Xu, M.J., Yu, D.Y., 2005. Terrestrial heat flow distribution in Kuqa forelandbasin, Tarim, NW China. Pet. Explor. Dev. 32, 79–83 in Chinese with English abstract.
Wang, P.W., Jin, Z.J., Pang, X.Q., Guo, Y.C., Chen, X., Guan, H., 2018. Characteristics of dual media in tight-sand gas reservoirs and its impact on reservoir quality: A case study of the Jurassic reservoir from the Kuqa Depression, Tarim Basin, Northwest China. Geol. J. 53, 2558–2568.
Wang, Q.C., Zhang, Z.P., Lin, W., 2004. Late Tertiary faults and their paleostress along the boundary between the Kuqa Basin and the Tianshan Mountains. Chin. Sci. Bull. 4, 374–381.
Wei, G.Q., Zhang, R.H., Zhi, F.Q., Wang, K., Yu, C.F., Dong, C.Y., 2021. Formation conditions and exploration directions of Mesozoic structural-lithologic stratigraphic reservoirs in the eastern Kuqa depression. Acta Petroleum Sinica 42, 1113–1125 in Chinese with English abstract.
Wygrala, B.P., 1989. Integrated study of an oil field in the southern Po Basin, Northern Italy. University of Cologne, Germany. PhD dissertation,.
Xiao, X.C., Liu, X., Gao, R., Houn, K., Luo, Z.H., 2001. Collision tectonics between the Tarim block (basin) and the northwestern Tibet Plateau: New observations from a moltidisciplinary geoscientific investigation in the western Kunlun mountains. Acta Geol. Sin. 75, 126–132.
Yang, S.F., Jia, C.Z., Chen, H.L., Wei, G.Q., Cheng, X.G., Jia, D., Xiao, A.C., Guo, S.J., 2002. Evolution of Tethys tectonic belt and formation of basin group in its northern margin and prospect of natural gas exploration in the Tarim Basin. Chin. Sci. Bull. 47, 36–43.
Yin, A., Nie, S., Craig, P., Harriso, T.M., Ryerson, F.J., Qian, X.L., Yang, G., 1998. Late Cenozoic tectonic evolution of the southern Chinese Tian Shan. Tectonics 17, 1–27.
Zeng, L.B., Wang, H.J., Gong, L., Liu, B.M., 2010. Impacts of the tectonic stress field on natural gas migration and accumulation: A case study of the Kuqa Depression in the Tarim Basin, China. Mar. Pet. Geol. 27, 1616–1627.
Zhang, L.K., Luo, X.R., Ye, M.Z., Zhang, B.S., Wei, H.X., Cao, B.F., Xu, X.T., Liu, Z.D., Lei, Y.H., Li, C., 2021. Small-Scale Diagenetic Heterogeneity Effects on Reservoir Quality of Deep Sandstones: A Case Study from the Lower Jurassic Ahe Formation. Eastern Kuqa Depression. Geofluids 1–25.
Zhao, G.J., Li, X.Q., Liu, M.C., Dong, C.Y., Chen, D.Y., Zhang, J.Z., 2022. Reservoir Characteristics of Tight Sandstone and Sweet Spot Prediction of Dibei Gas Field in Eastern Kuqa Depression. Northwest China. Energies 15, 3135.
Zhao, M.J., Lu, X.S., Zhuo, Q.G., Li, Y., Song, Y., Lei, G.L., Wang, Y., 2015. Characteristics and distribution law of hydrocarbon accumulation in Kuqa foreland basin. Acta Petroleum Sinica 36, 395–404 in Chinese with English abstract.
Zhao, W.Z., Zhang, S.C., Wang, F.Y., Cramer, B., Chen, J.P., Sun, Y.G., Zhang, B.M., Zhao, M.J., 2005. Gas systems in the Kuche Depression of the Tarim Basin: Source rock distributions, generation kinetics and gas accumulation history. Org Geochem. 36, 1583–1601.
Zhou, X.X., 2001. The mesozoic-cenozoic fluid pressure structure and reservoir-forming machine process in the Kuqa petroleum system in the Tarim basin. Earth Sci. Front. 8, 351–361.
Zhu, G.Y., Yang, H.J., Zhang, B., Su, J., Chen, L., Lu, Y.H., Liu, X.W., 2012. The geological feature and origin of Dina 2 large gas field in Kuqa Depression, Tarim Basin. Acta Petrol. Sin. 28, 2479–2492.
Zhuo, Q.G., Zhao, M.J., Li, Y., Wang, Y., 2014. Dynamic sealing evolution and hydrocarbon accumulation of evaporite cap rocks: an example from Kuqa foreland basin thrust belt. Acta Petroleum Sinica 35, 847–856 in Chinese with English abstract.
Zou, Y.R., Zhao, C.Y., Wang, Y.P., Zhao, W.Z., Peng, P., A., Shuai, Y. H.,, 2006. Characteristics and origin of natural gases in the Kuqa Depression of Tarim Basin, NW China. Org Geochem. 37, 280–290.